JTTEE 3:75-104

Measurement and Analysis of Adhesion Strength for Thermally Sprayed Coatings*

C.K. Lin and C.C. Berndt

Thermally sprayed coatings have a distinctive microstructure which can be described as "a three dimensional layered structure of discs which are interlaced to form a material of composite nature." The coatings are normally greater than 25 μm in thickness and can thus be described as bulk coatings. The minimum microstructural detail would be a single splat (ofter described as a lamella) which is about 5 μm (approximately 0.0002 in.) in thickness and up to 80 μm (approximately 0.003 in.) in diameter.

This paper focuses on methods used to define and measure the adhesion of coatings or deposits formed by thermal spray technology. The properties distinguished include strength and toughness. Measurements such as the tensile adhesion test (according to ASTM C633), the double cantilever beam test, and the scratch test are detailed to illustrate their relevance to present industrial practice. Acoustic emission studies have also been used to assess the "crack density function," a product of the number of cracks and crack size. Indentation techniques have been used to determine the fracture toughness of coatings and to demonstrate that the material properties of coatings are anisotropic. These techniques, among others, may be used to gain a fundamental understanding of coating performance or for quality control. A further focus of this paper concerns the highly variable nature of the material properties of coatings. Such variation leads to poor reproducibility during service and can cause unpredictable performance. Therefore, a section is presented on the statistical analysis of thermal spray coatings, with particular reference to the Weibull distribution.

1. Introduction

1.1 *Formation and Structure of Thermally Sprayed Coatings*

A VARIETY of thermal spray processes can be used to deposit thick coatings for a broad range of applications (Ref 1-3). These processes are essentially similar in that a material is heated by a gaseous medium and simultaneously accelerated and projected onto a substrate. The family of thermal spray processes includes flame spraying, plasma spraying, vacuum plasma spraying (also called low-pressure plasma spraying), high-velocity oxygen fuel (HVOF), arc metallization, and detonation gun spraying. The prime distinctions among these spraying processes are the temperature of the process and the velocity of the thermal source employed. These process variables control the nature of the materials that can be sprayed. The techniques also differ with regard to their process economics—that is, factors such as the cost of equipment, the cost of feedstock materials and other consumables (gases, grit blast media, etc.) that may limit the viability of a particular process. Several conferences have been devoted to thermal spraying, and the published proceedings (Ref 4-6) cover many of the processing variables associated with this technology.

Key Words: acoustic emission, adhesion measurement, confidence intervals, fracture mechanics, maximum likelihood estimation, statistical analysis, Weibull distribution

*Based on "Measurement of Adhesion for Thermally Sprayed Material," *Journal of Adhesion Science and Technology*.

C.K. Lin and **C.C. Berndt**, The Thermal Spray Laboratory, Department of Materials Science and Engineering, SUNY at Stony Brook, Stony Brook, NY 11794-2275, USA.

Thermal spray technology is not limited to coating substrates but also encompasses the manufacture of net shapes (Ref 7), which can be considered as very thick coatings (up to approximately 25 mm, or 1 in., in thickness) stripped from the substrate (or "forming tool") and then used directly as an engineered material (Ref 8). The availability of thermal processes enable the production of materials of varying composition and microstructure, the so-called functionally gradient materials.

Thermally sprayed coatings consist of a layered structure that is highly anisotropic, with individual splats oriented parallel to the substrate surface (Ref 9). A microstructural cross section of a thermally sprayed material is illustrated in Fig. 1, where unmelted particles are embedded within the layered structure and pores exist either totally within or between each layer (Ref 10). After formation of the coating, the first property criterion for this coating system is "How well is the coating adhered to the substrate?" and it therefore follows "How can we evaluate this adhesion strength, especially for coatings which are in service?". The intent of the following contribution is to describe and then discuss methods of measuring the "adhesion strength" of thermally sprayed coatings.

1.2 *Rationale for Adhesion Measurement*

According to Mittal (Ref 11), adhesion can be expressed in various ways. For example, "basic adhesion" signifies the interfacial bond strength and is the summation of all intermolecular or interatomic interactions. The result of an adhesion test is called "practical adhesion" and is a function of basic adhesion and a number of factors, all of which represent the work required to detach a film or coating from a substrate. Many theories and mechanisms for thermally sprayed coatings have been proposed (Ref 12, 13); none, however, covers all situations, and no adhesion test satisfies all requirements. Therefore, the best test method is often the one that simulates practical stress conditions.

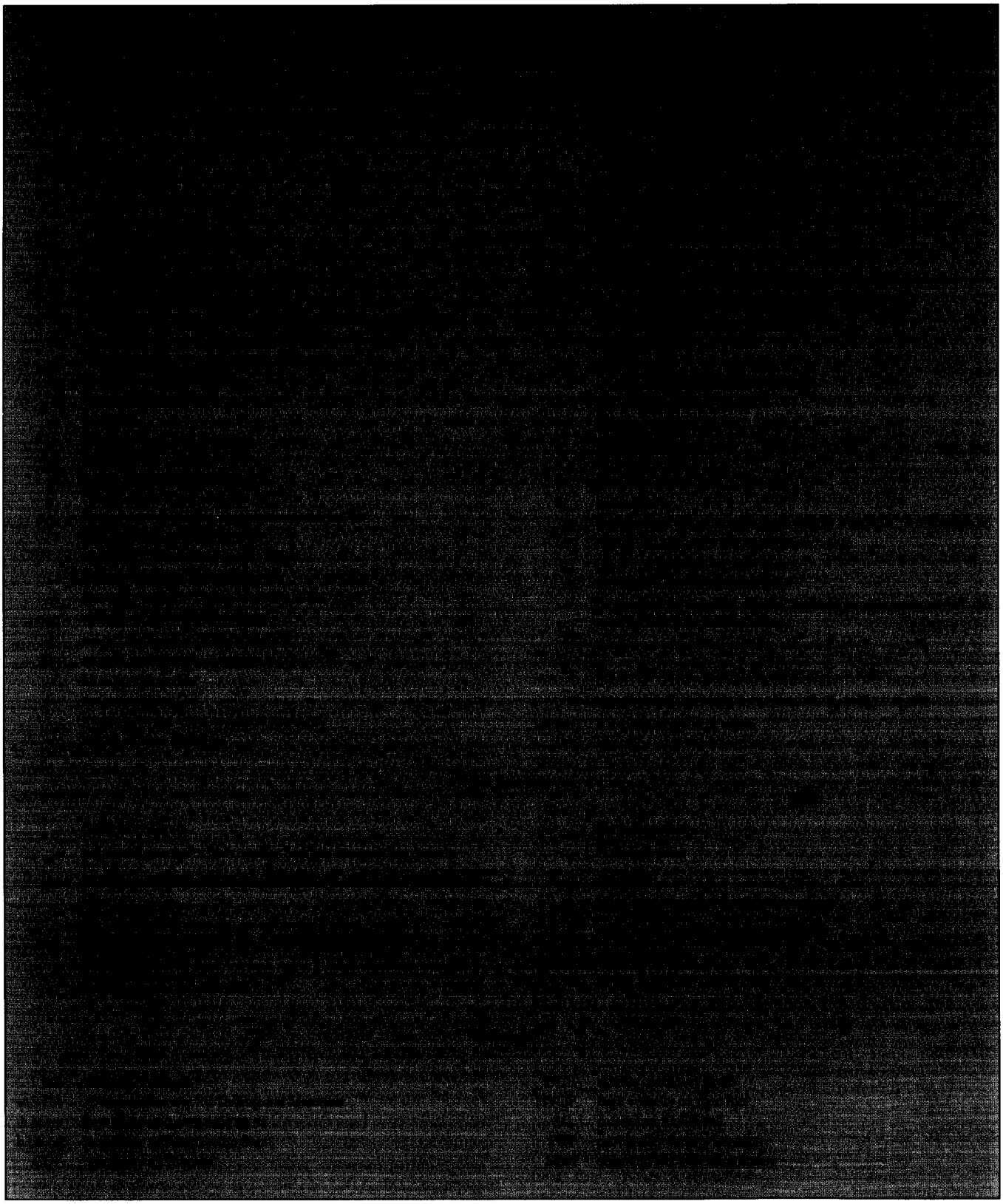

The term "adhesion" requires special definition for the purposes of thermal spray coatings. For example, ASTM defines adhesion as "the state in which two surfaces may consist of valence forces or interlocking forces or both" (Ref 14). Theories of adhesion between two materials generally include mechanisms based on diffusion, mechanical interlocking, electrostatic attraction, physical adsorption, chemical bonding, and weak boundary layers (Ref 15). However, the above global definition

be applied to thermal spray materials, because these coatings can be considered as "composites" at the microstructural level. Thus, bonding mechanisms for forming an integral coating or net shape will also be complex and may involve adhesion processes that are exclusive of those established for classical joining technology. The basic bonding mechanisms that have been defined for thermal spray coatings can be categorized into three major groups: (1) mechanical interlocking or anchoring, (2) metal-to-metal bonding, and (3) chemical bonding (formation of an intermetallic compound with a substrate) (Ref 16).

The specific thermal spraying process will influence the microstructure of the coating, and thus it can be inferred that the adhesion strength of the deposit will vary. For example, the HVOF technique produces a very dense microstructure with porosity typically less than 2%, compared to the less than 5% porosity for a flame-sprayed or an atmospheric plasma-sprayed material. Thus, factors affected by the spray parameters, including the size and distribution of porosity, oxide content, residual stresses, and macro- or microcracks, influence the performance of a coating system. A coating system may include several materials (polymers, metals, and/or ceramics) in a heterogeneous layered-type structure or as a composite mixture in which several material phases are dispersed. A substrate that is surface prepared and preheated also plays an important role in coating integrity because it is a platform for the transmission of operational stresses.

The service failure mode can be described as interfacial, cohesive, or mixed interfacial/cohesive.* Laboratory tests must induce the observed service failures; otherwise, such tests will be of limited application to engineering design and quality control. Useful measurements of adhesion strength and interpretation of test results to predict the service life of coatings or net shapes are the most challenging problems facing thermal spray scientists.

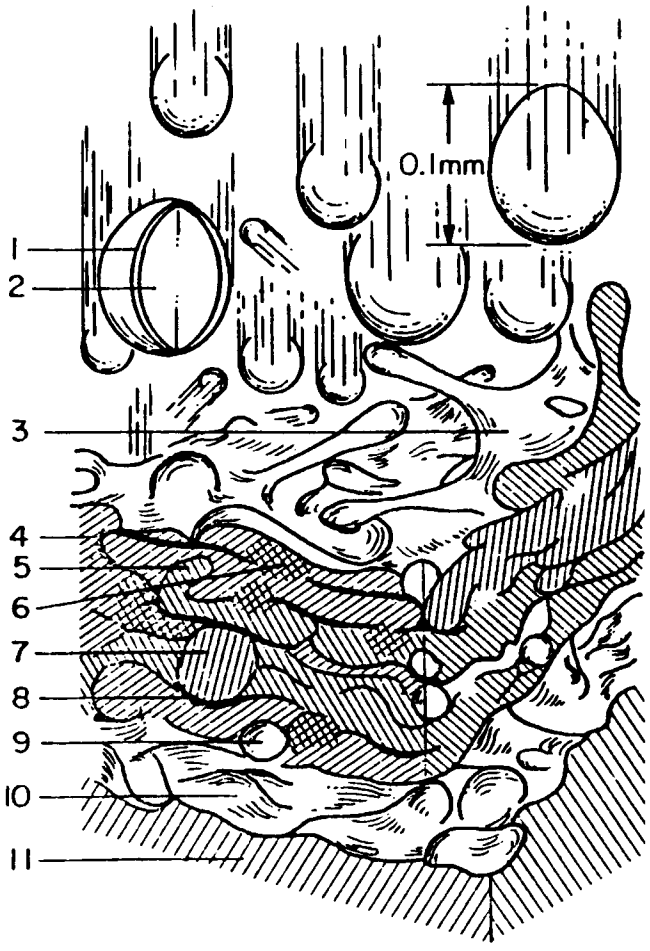

Fig. 1 Schematic cross section of the microstructure of thermally sprayed coatings. 1, partially sectioned oxide layer formed on a metal droplet in flight; 2, metal particle with its center still in the liquid state; 3, impinging metal droplet, partially splashing away; 4, burst oxide sheet situated between two metal layers; 5, interconnection (keying) of two particles that have splashed out; 6, partial alloying of two simultaneously impinging particles; 7, encapsulated presolidified spherical particle; 8, microcavity formed by uneven flow of splatted particles; 9, micropore caused by entrapped gases; 10, bond layer with roughened (grit-blasted) surface; 11, substrate material. Source: Adapted from Ref 10

1.3 *Application of Fracture Mechanics to Adhesion Measurement*

The adhesion of thermally sprayed coatings is not only an interfacial problem of each lamella within a coating, but also involves the integrity of the interface between the substrate and coating, residual stresses, crack population, and pore size and distribution. Fracture mechanics (Ref 17, 18) considers the energy required to initiate or propagate cracks and evaluates the adhesion of the coating system in terms of fracture toughness (Ref 19-21). Four-point bending methods, single-edge notched specimens, double cantilever beam (DCB) tests, indentation techniques, and other measurements have been employed to assess the adhesion of coating systems (Ref 22-24).

The purpose of all these methods is fundamentally the same when they are expressed from the viewpoint of fracture mechanics. The experimental proposition is to establish the equilibrium condition where the elastic energy provided by an external force (as defined by the geometry of the specimen and the applied load) is balanced by the propagation of a *stable* crack. One form of this energy-balance criterion derives the strain energy release rate, G (in J/m^2), and is defined as:

$$G = \frac{\partial(W_e - U)}{\partial A} \quad \text{(Eq 1)}$$

where W_e is work done by external forces (J), U is elastic energy stored in the system (J), and A is crack area (m^2). It is convenient to write G as:

$$G = \frac{P^2\, dC}{2B\, da} \quad \text{(Eq 2)}$$

where P is the force required to extend a crack (N), a is crack length (m), B is thickness (m), and C is compliance (m/N). The strain energy release rate can be related to the fracture toughness, K, by:

*The term "interfacial" is preferred over "adhesive" to avoid confusion with "an adhesive" used to join materials; that is, *adhesive* is used as a noun rather than as an adjective in this paper.

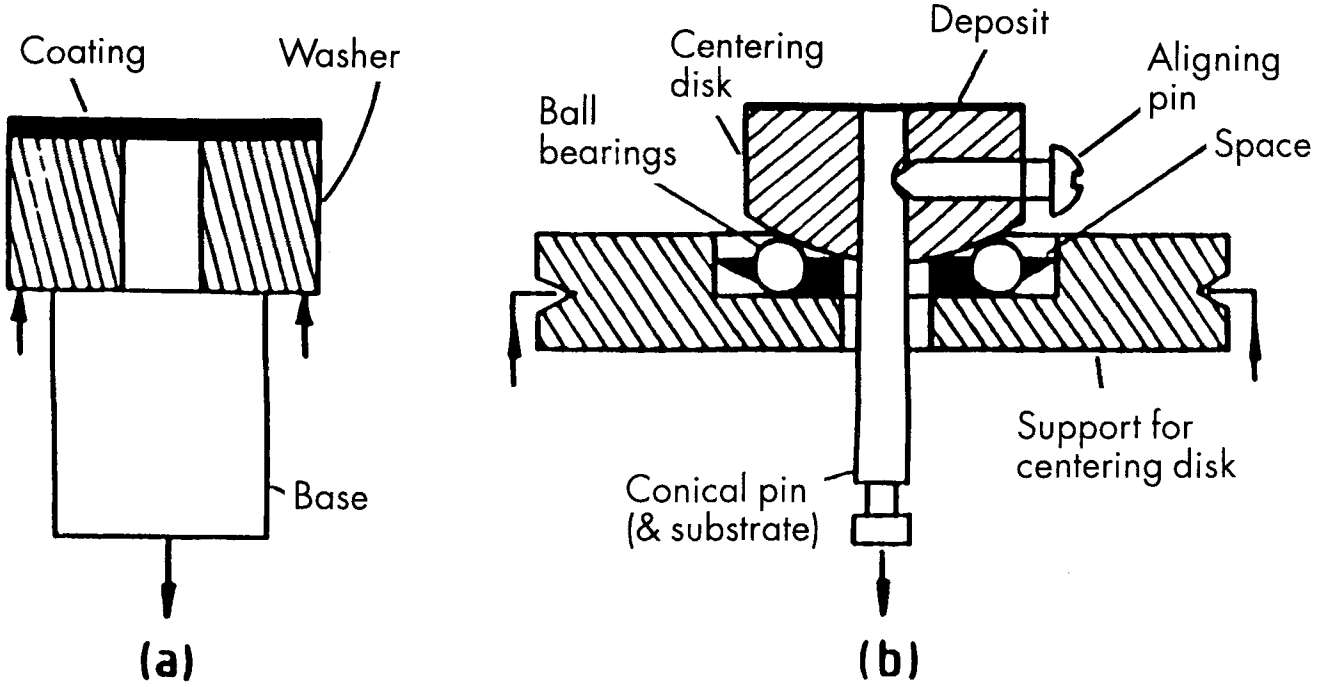

Fig. 2 (a) Specimen for determining adhesion strength. (b) Centering device and specimen in cross section. Source: Ref 28

Table 1 Methods for determining coating/substrate adhesion

Qualitative	Quantitative
Mechanical methods	
Cellophane tape test	Direct pull-off method
Abrasion test	Laser spallation test
Bend and scratch test	Indentation test
	Ultracentrifugal test
	Scratch test
Nonmechanical methods	
X-ray diffraction	Thermal method
	Nucleation test
	Capacitance test

$$K = \sqrt{\frac{EG}{1 - \nu^2}} \qquad \text{(Eq 3)}$$

where E is elastic modulus (MPa) and ν is Poisson's ratio.

When G exceeds a critical value, G_c, crack propagation occurs and failure of the coating system results. The evaluation of K with Eq 3 assumes that both the elastic modulus and the Poisson's ratio of the material are known; this is often not the case. The physical representation of the above equations is that the change in compliance of the specimen controls the energy input into the creation of new fracture surfaces. Thus, the corollary of this theory is that the crack path and rate of crack growth can be controlled precisely by appropriate design of the specimen. It now becomes possible to assess the tolerance of thermal spray coatings to cracks by measuring their fracture toughness.

Therefore, "mechanical adhesion" can be evaluated in terms of adhesion strength or fracture toughness. Such measurements of coating/substrate adhesion are listed in Table 1 (Ref 25-27). However, test methods for thermally sprayed coatings are restricted. The techniques to be discussed in this paper include the DCB test, the double torsion test, the bending test (three or four point), the scratch test, acoustic emission (AE) technology, and microhardness assessment.

2. Adhesion Measurements

One difficulty with any mechanical property assessment of coatings involves attachment of a loading device to the coating without influencing the property that is being measured. Some investigators (Ref 28) have approached this problem by manufacturing a pin or disk that can be removed from a mating component (Fig. 2). The surface of the assembly is thermally sprayed and then the pin or disk is removed. The force at fracture is used to find a parameter termed the "adhesion strength" of the coating. The corresponding shear test is performed by spraying the outside diameter of a cylinder or the head of a pin (Fig. 3) (Ref 29). One potential difficulty with the above test involves the duplex nature of the specimen assembly, which may influence the coating quality because the heating and cooling behavior of the deposit will be affected by the interface between the two components. Another feature of both the tensile and the shear tests is that the fracture mode is ambiguous, because mixed-mode failure often occurring. Mixed-mode failure, where a single fracture surface exhibits both interfacial and cohesive components, is a major practical obstacle in coating development. The inability to perform simple tests that reflect distinct (i.e., single) fracture morphologies makes the physical interpretation of current adhesion tests difficult.

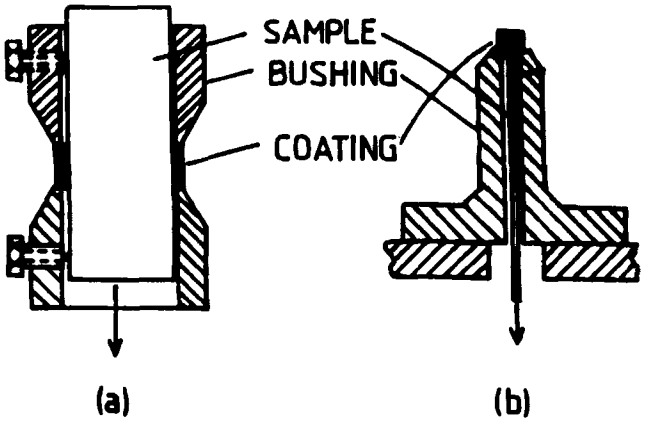

Fig. 3 Shear tests in which a bushing arrangement is used to apply a load in parallel to the coating lamellae. Source: Ref 29

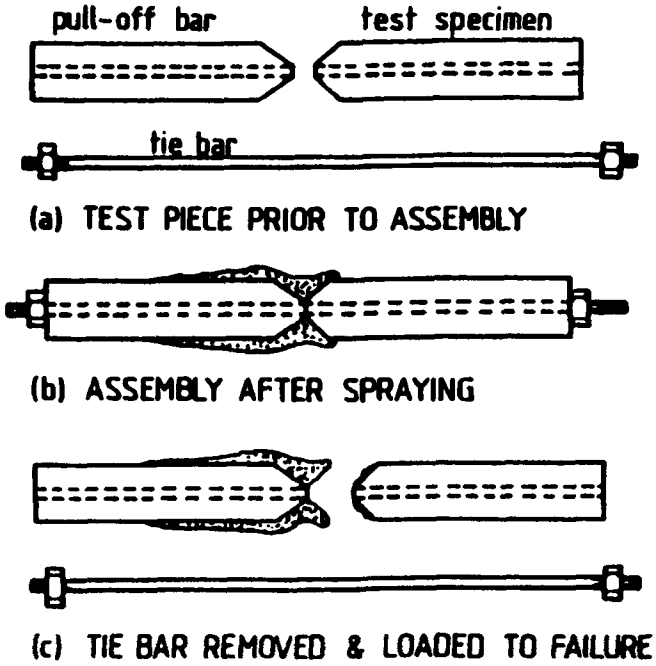

Fig. 4 Adhesion test piece that does not incorporate a glue. Source: Ref 30

Other geometries that do not require an adhesive (Fig. 4 and 5) have not been widely implemented outside their laboratories of origin. The method of spraying two adjoining conical parts is expected to incorporate a failure that has a large shear component (Fig. 5a), whereas the other shear test may exhibit shear failure either parallel to the substrate surface or through the coating thickness (Fig. 5b). Therefore, these tests, in common with other tests, do not manifest distinctive failure modes, which limits their universal application.

The adhesion properties of coatings were investigated on the microscopic level (Ref 32) by shearing individual particles from the substrate surface (Fig. 6). This study considered that adhesion to the substrate arose from interactions across the particle/substrate interface, and a strength of growth rate constant, K′, was defined as:

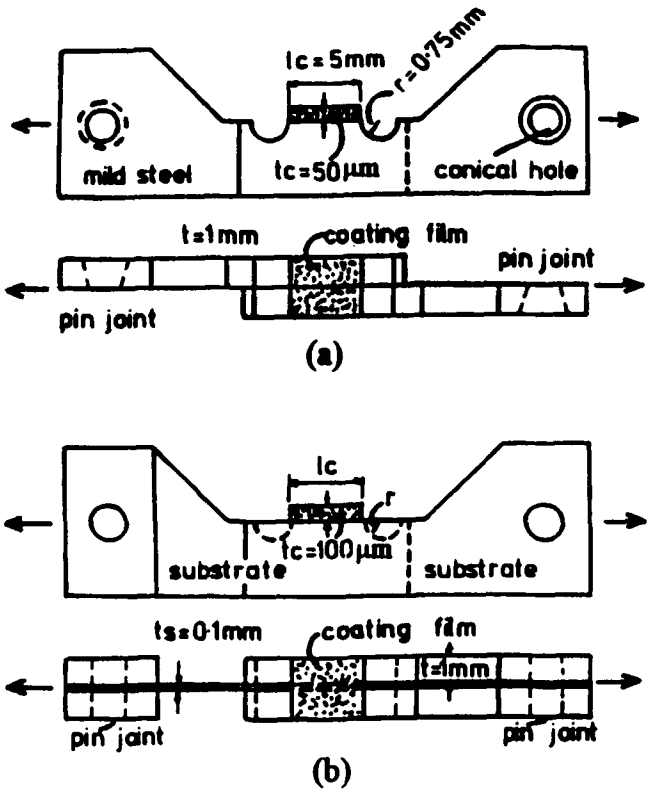

Fig. 5 Specimen configurations for determining coating adhesion. (a) Shear stress deformation. (b) Critical shear stress of adhesion. Source: Ref 31

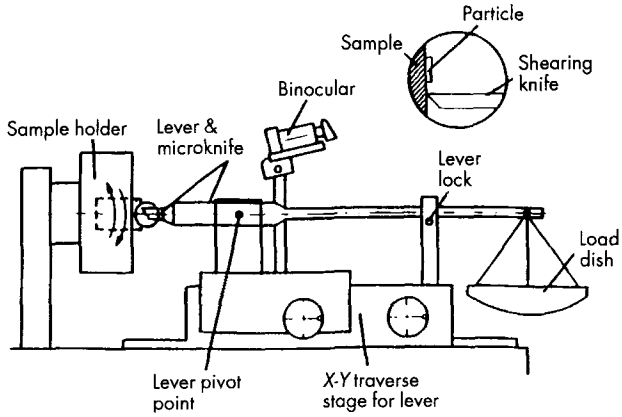

Fig. 6 Instrument for measuring the adhesion strength of particles. A microknife applies a shear load to individual particles. Source: Ref 32

$$K' = -\frac{1}{t} \ln \left(1 - \frac{N(t)}{N_o} \right) \quad \text{(Eq 4)}$$

where t is time, $N(t)$ is the number of atoms that react during the interaction time, and N_o is the number of atoms in the particle and substrate that are in contact.

The upshot of this analysis was that the strength of the coating at some interaction time of t was compared to the maximum strength of the coating at the end of the thermal spray process. It was established that the extent of the particle/interface reaction increased with both increasing particle pressure and tempera-

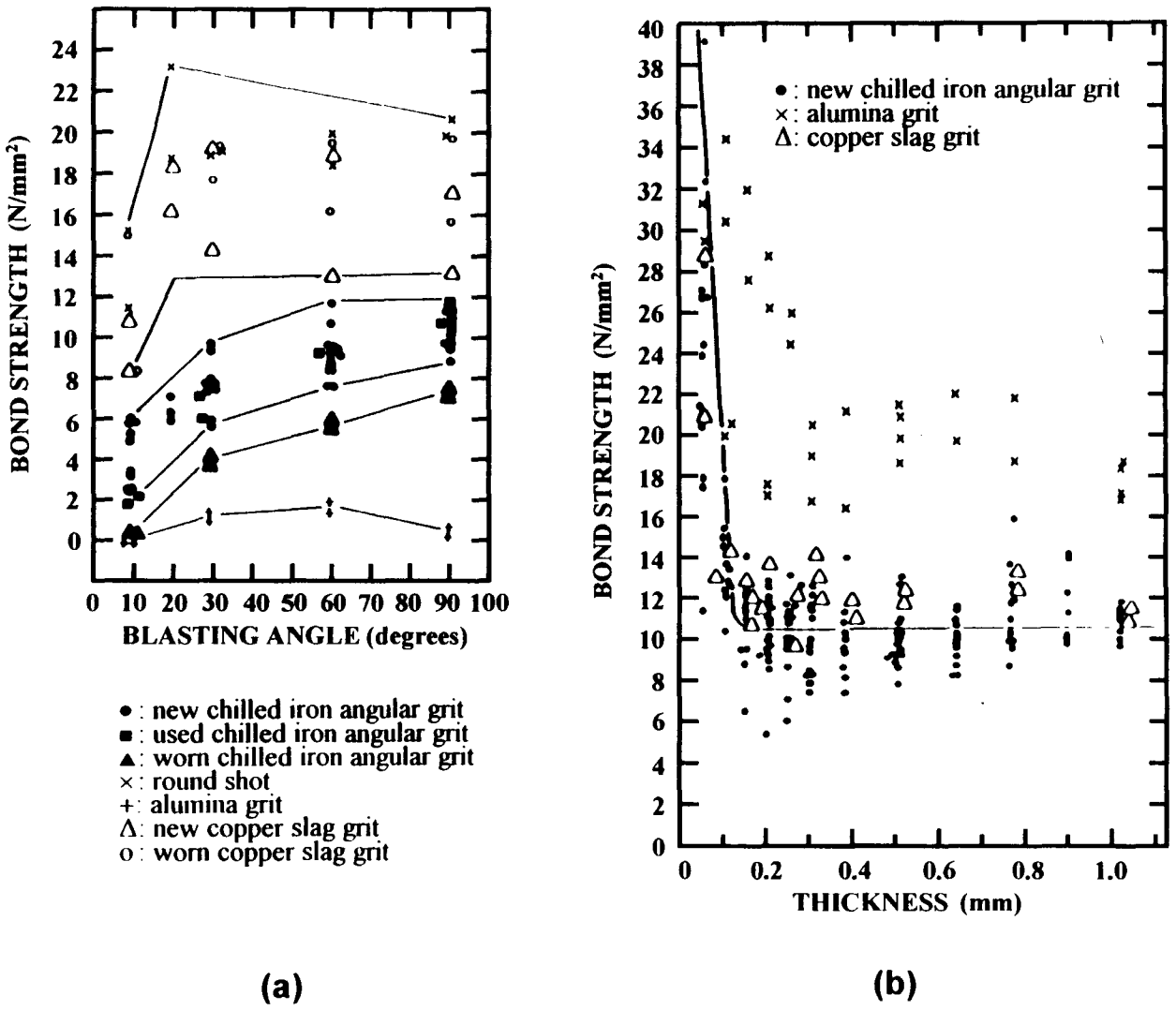

Fig. 7 Variation of bond strength of aluminum coatings after surface preparation with various media. The effects of (a) blasting angle and (b) coating thickness are indicated. Source: Ref 34

ture; this agreed with experimental observations that coating adhesion also increased under these conditions. Further theoretical work (Ref 33) has treated adhesion as a stochastic process that depends on the formation characteristics of the first monolayer of material. The coating buildup is treated as a statistical process involving input data from the thermal spray processing parameters, such as relative motion between the torch and substrate (i.e., the spray pattern), the velocity and temperature distribution of the thermal source, and the particle size.

The reason for performing adhesion measurements can be brought into focus by examining how such experiments are used to ascertain the utility of coatings. For example, bond strength measurements allow optimization of different grit-blast media and the angle of grit blasting as well as determination of the best thickness for aluminum coatings (Fig. 7) (Ref 34). Other workers (Ref 35) have optimized ceramic compositions and plasma spraying parameters with respect to strength. In recent years, with the adoption of design of experiment methods (Ref 36), bond strength measurements along with other physical measurements (roughness, electrical resistance, porosity, etc.) have been used to select coatings for industrial applications.

The adhesion measurement can be taken as a control parameter to optimize the many process parameters that are involved during thermal spraying. For example, the test can be used to establish the significance of process-induced residual stresses on coating integrity. Often the tensile adhesion test (TAT) is performed as a quality control test; numerous references can be found in thermal spray conference proceedings (Ref 4-6).

2.1 *Tensile Adhesion Test*

The TAT has been used widely as a routine quality control tool for thermal spray coatings. The TAT arrangement is illus-

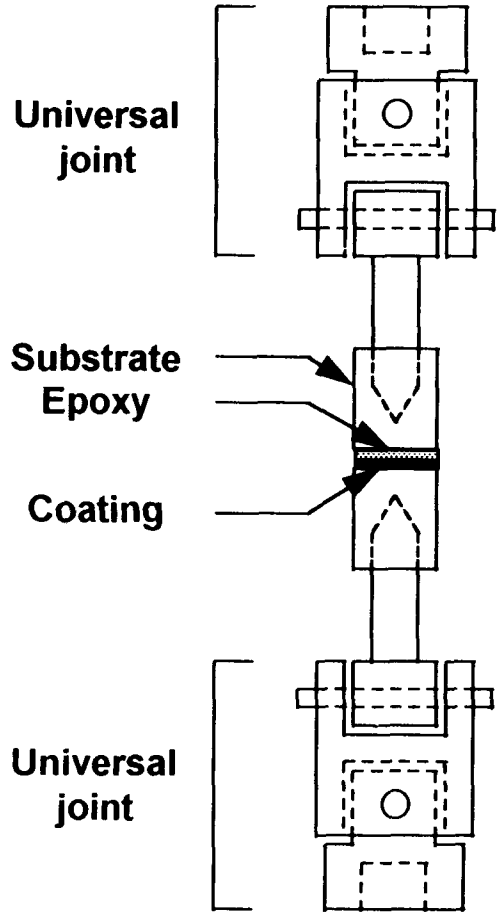

Fig. 8 (a) Tensile adhesion test configuration specified by ASTM C633-79.

trated in Fig. 8; at the center, a coated specimen is attached to a support fixture by epoxy so that a tensile force can be applied. The stress at failure is called the tensile adhesion strength or bond strength and is an important property for characterizing coatings. However, the TAT procedure has several shortcomings, including the penetration of epoxy and alignment of test fixtures. Mixed-mode failure may also occur, making the interpretation of results difficult.

Four main standards are used in industry or research: DIN 50160-A (Germany), AFNOR NF A91-202-79 (France), JIS H8666-80 (Japan), and ASTM C633-79 (USA). These standards differ in their specimen geometry, test methodology, and failure analysis (Table 2) (Ref 37). Shimizu et al. (Ref 38) have compared the differences between ASTM C633 and JIS H8666 and have found that coating strength appears to increase with a decrease in the ratio of coating thickness over the specimen diameter, presumably due to epoxy penetration to the substrate or changes in stress transfer across the coating.

The failure modes of a coating under TAT conditions are (1) interfacial failure, which occurs along the coating/substrate interface, (2) cohesive failure within the coating, and (3) mixed-mode failure, which is a combination of the first two modes. It is usually assumed that failure is controlled only by the magnitude of the applied tensile force, and therefore the average failure stress is measured. However, the highly defective nature of a thermal spray coating gives rise to stress singularities within the coating during a TAT. Recently, Han et al. (Ref 39) used finite-element analysis to study the stress distribution along the coating/substrate interface and found that the stress distribution was nonuniform and that the average adhesion strength was underestimated. A modified specimen, 50% longer than the standard size, was proposed so that a uniform stress can be obtained along the interface. A fracture mechanics approach was used to estab-

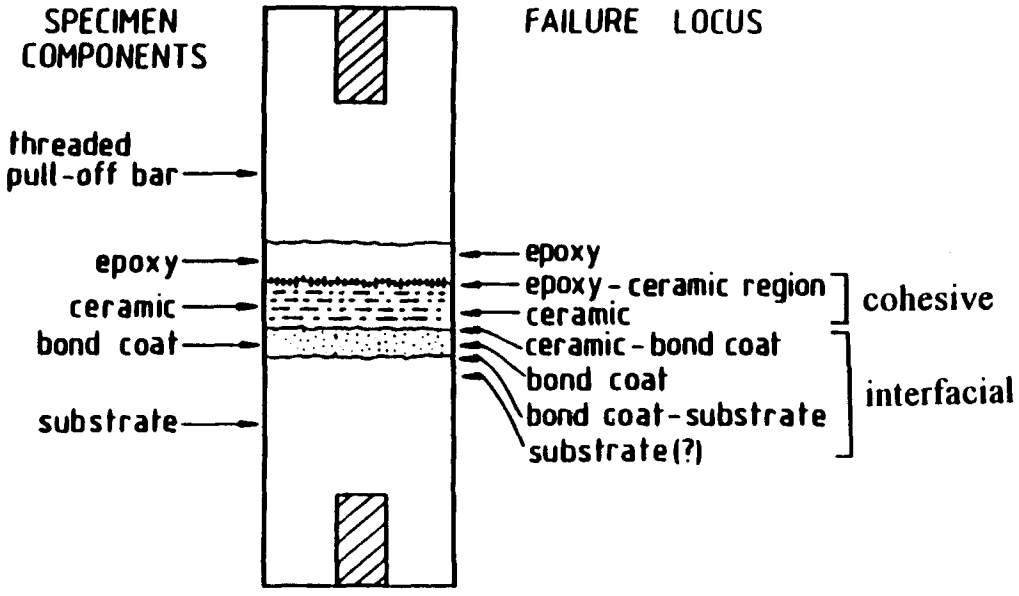

Fig. 8 (b) Tensile adhesion test specimen arrangement and possible failure modes

lish a relationship between the bond strengths determined from the standard and modified specimens, that is (Ref 40):

$$\sigma^e_{cr} \cong 1.21\ \sigma^s_{cr} \qquad \text{(Eq 5)}$$

where σ^e_{cr} is the bond strength of the elongated specimen and σ^s_{cr} is the bond strength of the standard specimen. Therefore, the standard ASTM C633 test is underestimated by a factor of 1/1.21 (~83%) due to stress singularities at the specimen edges. The factor of 1.21 in Eq 5 is independent of coating modulus, thickness, and Poisson's ratio.

The TAT data can also be analyzed according to fracture mechanics concepts, where the specimen configuration for the TAT geometry is considered as a circumferentially cracked bar (Fig. 9) (Ref 41). The average fracture strength can be converted into fracture toughness by:

$$K_{IC} = P\left[-1.27 + 1.72\left(\frac{D}{d}\right)\right]D^{-3/2} \qquad 0.4 \le \frac{d}{D} \le 0.9 \qquad \text{(Eq 6)}$$

where K_{IC} is the critical fracture toughness (N · $m^{-3/2}$, P is the fracture force (N), D is the outside diameter of the bar (0.0254 m), and d is the inside diameter in the circumferentially notched bar (m).

Data presented by Hermanek (Ref 42) have been analyzed using this concept (Ref 43) to find an estimation of the naturally occurring defects of a TAT specimen. The columns of "old" ratios presented in Table 3 can be transformed into area ratios that represent the effective reduction in average load-bearing area of the TAT specimen due to defects. The unsealed coatings (data sets 1 and 3) best represent current industrial practice, and the average reduced-area ratios range between 0.74 and 0.86. This reduction in area corresponds to a reduced failure stress of about 80%, which correlates reasonably well with the underestimation factor of approximately 83% found by Han et al. (Ref 40).

2.2 *Fracture Mechanics Approach*

The fracture mechanics approach to the evaluation of crack propagation is based on defining adhesion in terms of a stress-intensity factor, K, or strain energy release rate, G. Methods of measurement include the DCB test, double torsion test, bending test (three or four point), single-edge notched test, and compact tension test, and so on.

Table 2 Summary of major TAT specifications

	Test specimen		Testing conditions				
Standard specification	**Diameter, mm**	**Length, mm**	**Coating thickness, mm**	**Load rate, N/min**	**Crosshead displacement**	**Minimum number of tests**	**Failure description**
ASTM C 633-79	25.15-25.4	25.4	>0.38	...	0.013-0.021	5	Interfacial Cohesive(a) Epoxy(a)
DIN 50160-A	40 ± 0.1	50	>0.15 and <0.4(b) or <0.8(c)	1000 ± 100	...	5	Interfacial Cohesive
AFNOR NF A91-202-79	39.9	45	>0.5	1000 ± 100	...	6	Interfacial Cohesive Special cases
JIS H8666-80	25-40	40	>0.3 and <0.5	9806.6	0.017	...	Interfacial Cohesive Coating/epoxy

(a) Mixed-mode failures are of no practical use. (b) For oxides and carbides. (c) For metals. Source: Ref 37

Table 3 Fracture toughness values calculated from TAT results(a)

Data set(b)		**Average K_{IC}, MN · $m^{-3/2}$**	**Maximum K_{IC}, MN · $m^{-3/2}$**	***D/d*(c)**	**Maximum stress(d), MPa**	**Maximum K_{IC}(d) MN · $m^{-3/2}$**	***D/d*(e)**	**Difference(f), %**
Epoxy 1	A	1.56	2.01	0.93	44.7	2.52	0.86	25
	B	1.65	2.37	0.90	50.1	2.82	0.84	19
	C	1.81	2.70	0.89	55.5	3.12	0.84	16
Epoxy 1 plus sealer	A	1.46	2.38	0.86	47.2	2.66	0.82	12
	B	1.28	1.71	0.92	39.8	2.24	0.84	31
	C	1.39	2.62	0.81	43.9(g)	2.47	0.83	–6
Epoxy 2	A	0.81	1.14	0.90	22.4	1.26	0.87	10
	B	0.86	1.40	0.86	29.8	1.68	0.80	20
	C	1.90	2.50	0.92	48.2	2.71	0.90	9
Epoxy 2 plus sealer	A	0.73	1.28	0.83	24.1	1.36	0.82	6
	B	0.57	1.32	0.75	23.7	1.33	0.74	1
	C	0.34	0.52	0.88	10.5	0.59	0.84	14

(a) Original data from Ref 42. (b) A, B, and C represent three different manufacturers. (c) Calculated from the experimental maximum K_{IC} and the average stress value. (d) Theoretical values. (e) Calculated from the 99% percentile of the average stress value. (f) Difference between the calculated maximum stress and the experimentally determined high stress; expressed as a percentage of the experimental value. (g) Note that the calculated maximum stress is less than the experimentally determined stress. Source: Ref 43

The fracture mechanics mode of failure is a material property that not only can be controlled (to some degree) but that also must be quantified for engineering design purposes. Thus, a major justification for a fracture mechanics test is that a mode I (tensile) or a mode II (shear) test can be performed and the response of preexisting flaws ascertained. It is also possible to carry out mixed-mode tests, which may better replicate the variety of service conditions that the coating will experience throughout its lifetime.

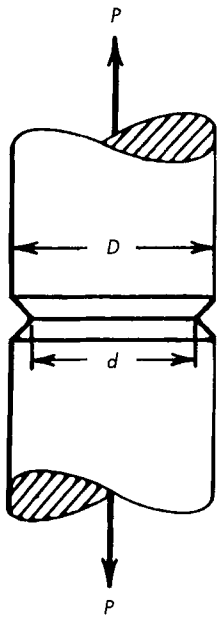

Fig. 9 Tensile adhesion test specimen of a circumferentially cracked bar for K_{IC} testing. Source: Ref 41

2.2.1 Double Cantilever Beam Test

A major advantage of the DCB test is the wide applicability offered to the design engineer; however, this ideal comes at the expense of more complex specimen preparation and sophisti-

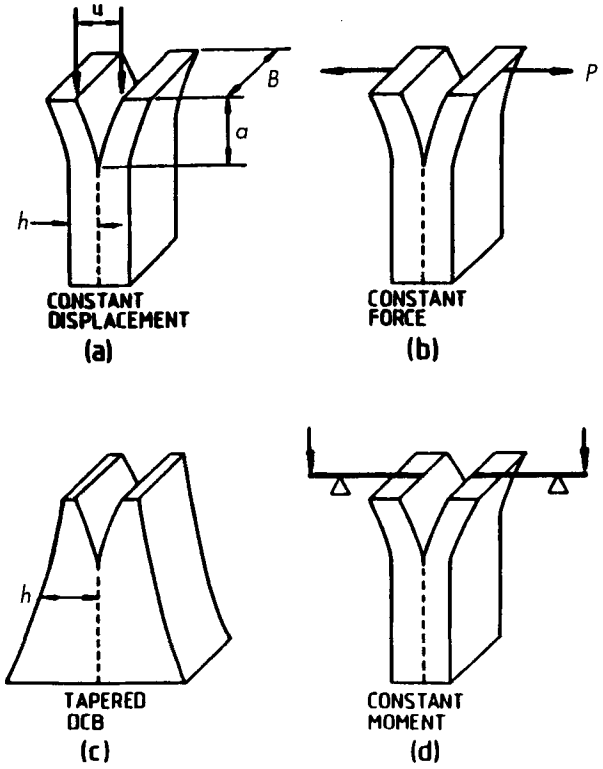

Fig. 10 Double cantilever beam test pieces

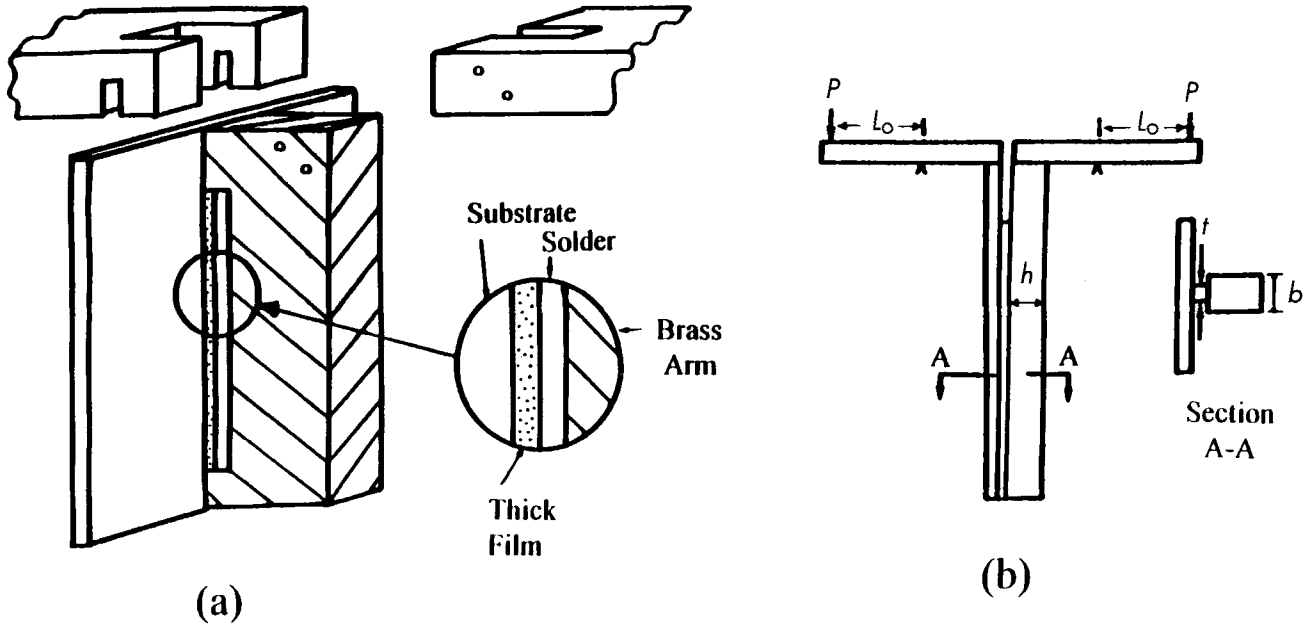

Fig. 11 Applied-moment DCB specimen for measuring the adhesion of thick films. (a) Specimen preparation. (b) Testing arrangement. Source: Ref 44

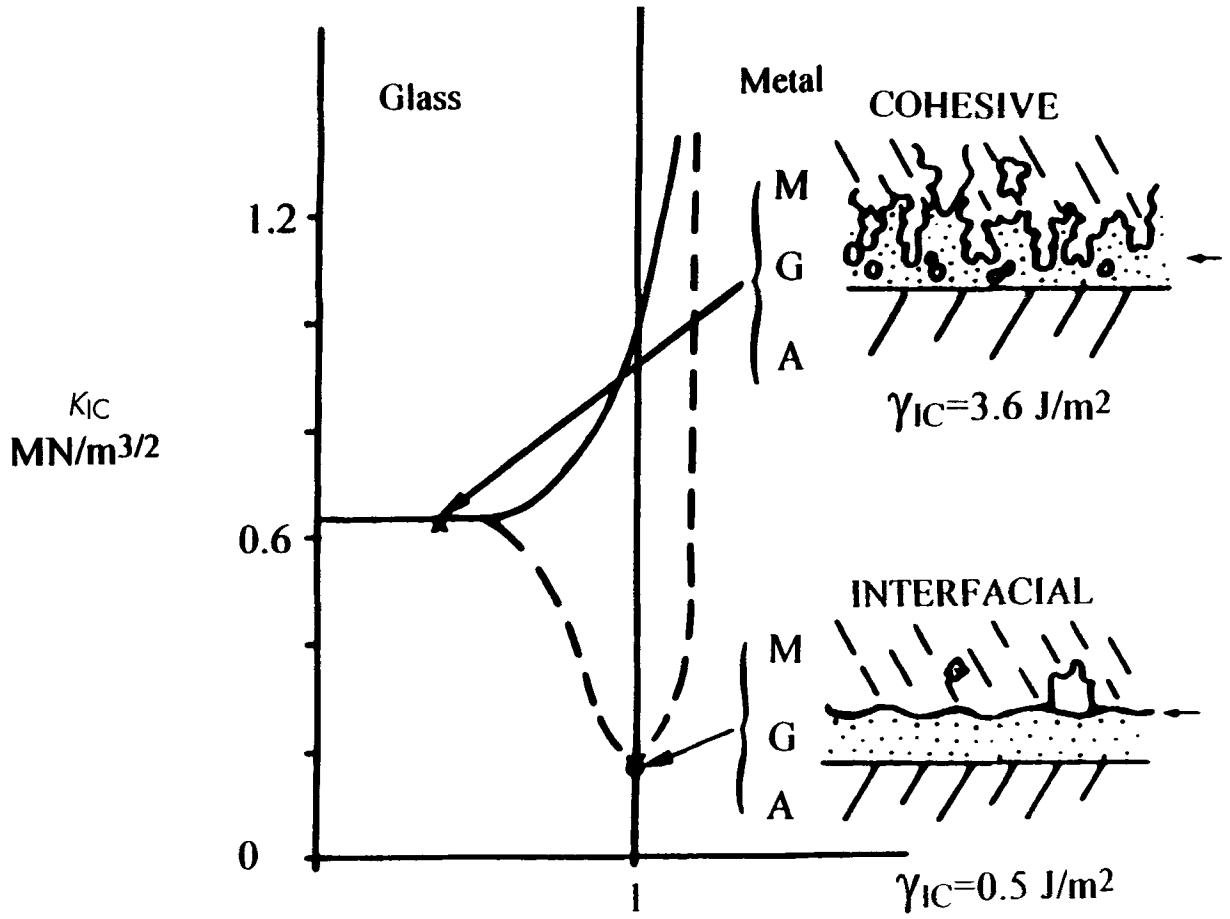

Fig. 12 Model of stress-intensity profile through film and substrate. M, metal; G, glass; A, alumina. Source: Ref 45

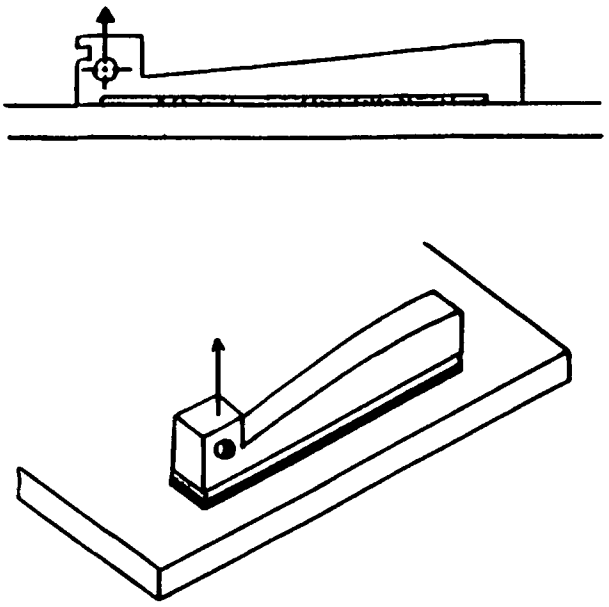

Fig. 13 Specimen with DCB geometry in which one arm is contoured. Source: Ref 46

cated experimental techniques than the quality control departments of thermal spray shops may be prepared to undertake.

Many configuration of this test are available (Fig. 10); an example of the technique on a thick-film conductor of alumina is shown in Fig. 11 (Ref 44) . The applied-moment method was used in this case, because the crack length, a difficult property to measure for these opaque coatings, was not required. These studies (Fig. 12) (Ref 45) are analogous to those on thermal spray coatings where interfacial and cohesive modes of failure were distinguished in terms of fracture toughness. Another DCB geometry arrangement is illustrated in Fig. 13 (Ref 46), where a single contoured arm is used.

The general nature of the force versus displacement (i.e., F versus μ) requirement of a DCB experiment is shown in Fig. 14. The elastic energy of the specimen arms determines the amount of energy that is transferred to the creation of new crack faces within the locus of fracture. Thus, crack growth, as indicated by the dashed line in Fig. 14, will continue until a stable condition is reached; crack propagation stops at that point. The new slope of the force/displacement curve (i.e., the compliance) indicates the magnitude of the new crack length, and the area enclosed within the force/displacement curve is related to an energy transfer (from the DCB arms to the crack) during crack growth. Thus,

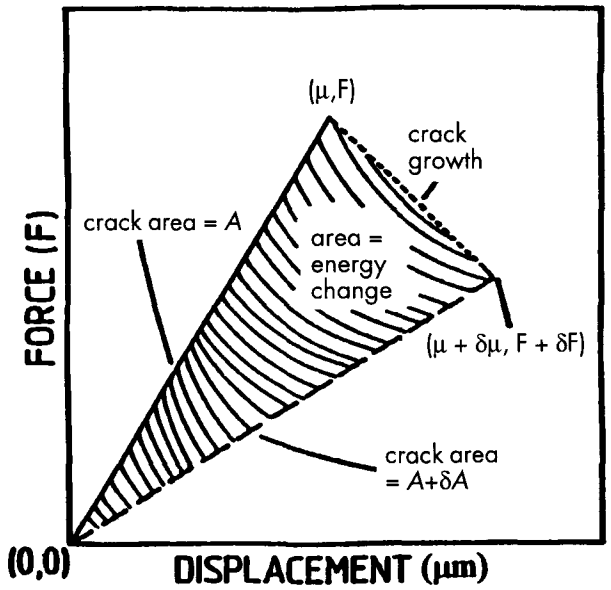

Fig. 14 Energy change when a crack grows during a DCB test. F, force; μ, displacement

the versatility of the DCB method is that the energy input into the coating can be controlled by altering the elastic modulus and/or geometry of the DCB arms.

It is also necessary to verify that the arms of the DCB are indeed bending and that there is no rigid movement of the adherents (Fig. 15a). It was established (Ref 22) that true bending of the DCB arms did take place as shown in Fig. 15(c), rather than the ideal situation depicted in Fig. 15(b). The composite DCB geometry, which incorporated an adhesive joint, did not directly obey the Mostovoy formulation (Ref 47); however, a modified equation that incorporated displacement at the crack tip and deformation beyond the crack tip fitted reasonably well to the theory (Fig. 16).

2.2.1.1 *DCB Test for Thermally Sprayed Materials*

In the basic DCB test on coatings (Fig. 17), a tension force is applied to the specimen assembly and displacement is measured by an extensometer placed on the arms (Ref 22). When cracking initiates, as evidenced by decreasing load with increasing extension, the DCB is unloaded. Several loading/unloading sequences are performed until the specimen completely fails, at which point the morphology can be examined by optical microscopy and scanning electron microscopy (SEM). Any of the three failure modes—interfacial, cohesive, or mixed—can be observed, and both interlamellar cracking and translamellar cracking are exhibited. The locus of fracture can be controlled by grooving the edges of the DCB, as shown at the right in Fig. 17. The DCB method is not limited by the strength of the adhesive, as is the case for tensile adhesion tests. However, because it is a fracture mechanics test, the fracture toughness of the adhesive must be greater than that of the coating. This condition is relatively easy to satisfy.

2.2.1.2 G_{IC} *Determination*

The critical strain energy release rate, G_{IC}, is determined from Eq 2. The compliance gradient values, dC/da, are determined from the displacement at the loading points, C_{LP}, which differs from the values recorded by the extensometer (termed the crack opening displacement, C_{COD}). An experimentally determined calibration curve is necessary to calculate dC/da (Ref 22, 48). Several researchers have used this technique to generate G_{IC} data; results are shown in Table 4. The mean G_{IC} values for ceramic coatings exhibit a wide range but generally can be considered to lie below approximately 100 J/m^2, whereas G_{IC} for metallic coatings is greater than 100 J/m^2. Typical G_{IC} values are 20 J/m^2 for bulk Al_2O_3 and 8000 to 30,000 J/m^2 for aluminum alloys.

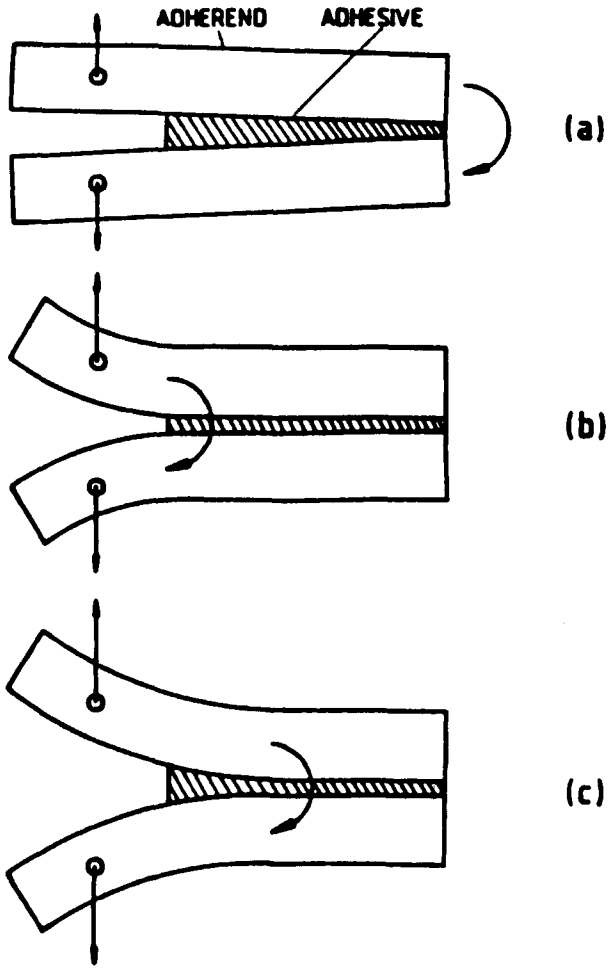

Fig. 15 Bending modes of DCB specimen. (a) Rigid arms. (b) Cantilever beams built in at the crack tip. (c) Rotation of cantilever beams at a point beyond the crack tip.

2.2.2 Double Torsion Test

The double torsion test (Ref 49, 50) has been applied to thermally sprayed coatings (Fig. 18). The prime advantage of this test is that the crack length need not be measured, because cracking occurs at a constant strain energy release rate or stress-intensity factor. Specimen manufacture involves incorporating the coating into an arrangement so that a torque can be applied to the crack front. A drawback of the test is that mode I cracking, where

Table 4 G_{IC} values for thermally sprayed coatings measured by the DCB method(a)

Material	Mean G_{IC}, J/m^2	Standard deviation	Failure	Ref
Al_2O_3	12	2	Interfacial	22
	16.1	5.3	Cohesive	23
	21	5	Cohesive	22
	31.6	9.3	Cohesive	23
	49.8	14.0	Cohesive	23
	52.7	14.5	Cohesive	23
	58	16	Interfacial bond coat	22
Al_2O_3-2.5TiO_2	15.9	5.6	Cohesive	23
Al_2O_3-40TiO_2	48.7	15.8	Interfacial	23
ZrO_2-10CeO_2	11.4	3.6	Interfacial	21
ZrO_2-15CeO_2	74.1	22.9	Interfacial	21
	125.4	51.1	Cohesive	21
ZrO_2-6Y_2O_3	49.9	16.7	Interfacial	21
	95.5	39.4	Cohesive	21
	148.3	52.3	Mixed	21
ZrO_2-20Y_2O_3	30.0	10.4	Interfacial	21
	69.7	31.8	Cohesive	21
	43.2	19.6	Mixed	21
ZrO_2-10CeO_2	11.4	3.6	Interfacial	21
Mild steel	116	21	Interfacial	22
	261	71	Cohesive	22
Ni-Al	319	95	Cohesive	22
Ni-20Al	362	16	Cohesive	23

(a) For data given in K, Eq 3 is used to convert K into G by assuming E = 48 GPa and ν = 0.25.

the crack front is orthogonal to the crack propagation direction, has not been verified for thermal sprayed materials. Also, practical experience has shown that both arms of the double torsion specimen deflect at a constant angle along their entire length. Both of these conclusions are reflected in the fracture surface morphology shown in the lower detail of Fig. 18, which illustrates a mixed mode of failure.

2.2.3 Bending Test

In the three-point bend test, a rectangular coupon is placed on two rolls and a third roll applies a load at the midspan location. During the test, the upper half of the specimen is under compression, while the complementary half is under tension. In the four-point bend test, two upper rolls are used to apply load, and thus a more uniform stress distribution is obtained. The four-point bend test is less sensitive to defects within coatings, because stresses are more homogeneously distributed over the test volume.

Four-point bend tests have been used to determine the adhesion of thermal spray coatings. Ferber and Brown (Ref 51) investigated the strength degradation of plasma-sprayed alumina coatings. The coatings were sprayed onto metallic substrates and adhered to the other load-bearing support by epoxy (Fig. 19). Fatigue experiments were performed to assess the effects of stress corrosion by measuring the time to failure. Strength degradation was observed within ceramic/metal systems, and the fatigue results were strongly influenced by the nature of the epoxy. Cox (Ref 52) measured the adhesion strength of detonation-gun coatings by performing four-point bend tests with simultaneous monitoring of the acoustic emission. The substrate assembly was loaded with the coating in tension. The strain was monitored and any cracking detected by AE so that the strain to fracture (STF) was determined. The STF parameter was dependent on the residual stress and exhibited little dependence on the hardness and metallic content of the coatings. Howard and Clyne (Ref 53) used the bimaterial notched four-point bending specimen (Fig. 20) to study the interfacial fracture toughness of vacuum plasma-sprayed titanium coatings. The cracks propagated under mixed-mode conditions. The interfacial fracture energy and critical stress-intensity factor were evaluated from the load-displacement data. The residual stress state of the coatings substantially affected crack propagation; for example, G_c was 6.79 $\pm$ 0.35 J/m^2 for coatings with residual stress and 2.98 $\pm$ 0.19 J/m^2 for coatings without residual stress. These values are much smaller than the material properties reported for other coatings.

The stress-intensity factor, K, is a function of applied load and specimen geometry. The calibration to obtain the relationship between K and specimen geometry is important; K calibrations are summarized in Table 5 (Ref 54).

2.3 *Scratch Test*

The scratch test, originally studied by Benjamin and Weaver (Ref 55), is often used to characterize thin, hard coatings such as TiN and TiC (Ref 56, 57). In this test, a loaded Rockwell C diamond stylus is drawn across the coating surface under either constant or gradually increasing load. In one variation of the test, the AE is also monitored during the scratching procedure so that the critical load, L_C, for failure can be measured. The failure morphology is examined by optical microscopy or SEM. If interfacial, cohesive, or mixed failure mode is observed, then L_C is used as a qualitative value of coating/substrate adhesion.

Three contributions to coating loss have been identified for the scratch adhesion test (Ref 58-61): an elastic/plastic indentation (a ploughing component), an internal stress component, and a tangential frictional stress (an adhesion component). Bull et al. (Ref 59) discussed the importance of frictional drag and sug-

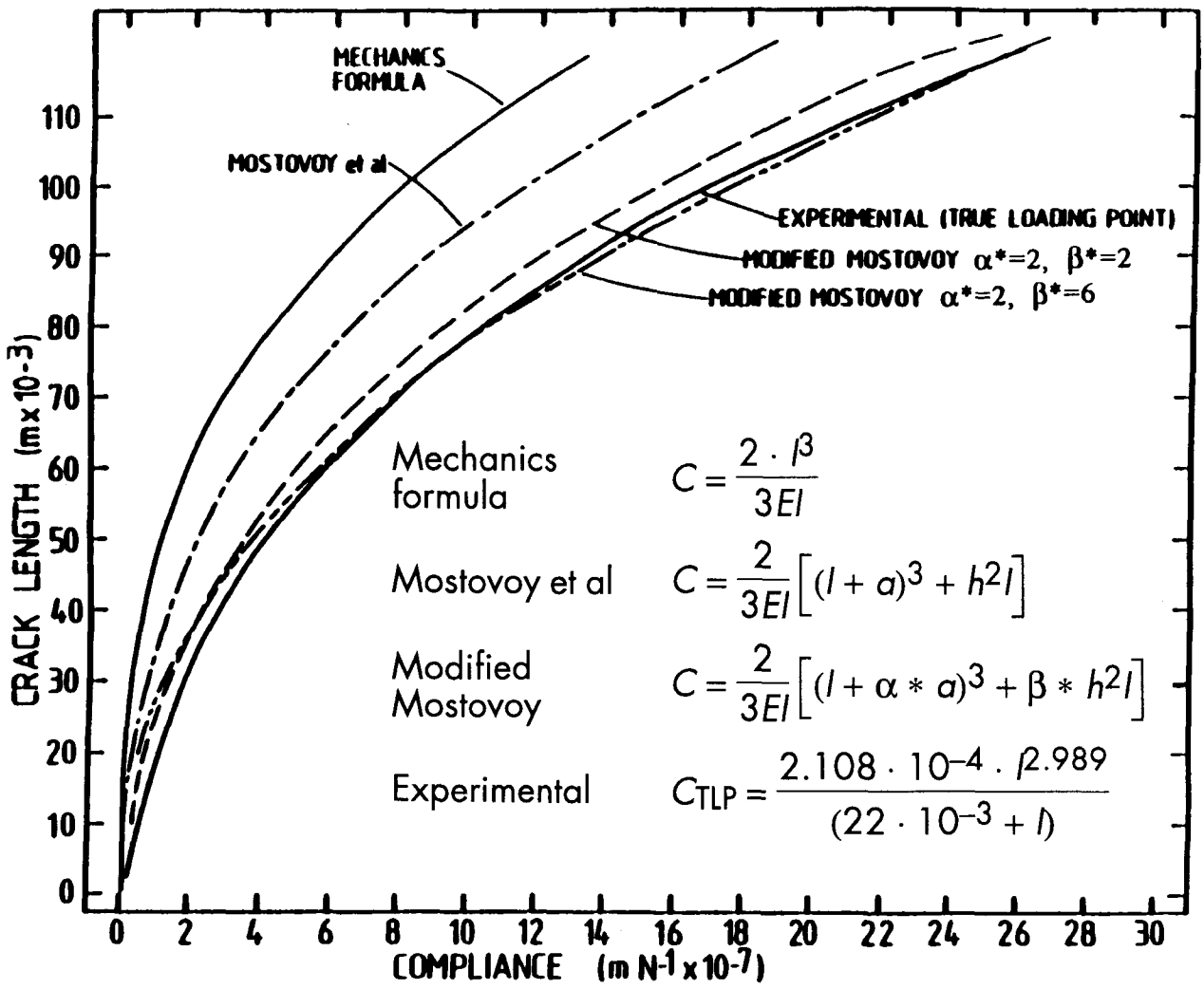

Fig. 16 Experimental compliance/crack-length functions compared to various theories that can be applied to the experimental data

Table 5 *K* calibrations for various specimen designs

Test method	Equation	Variables
Three-point bending	$K_I = Y\frac{3Pl\sqrt{a}}{2BW^2}$ $Y = 1.93 - 3.07\left(\frac{a}{W}\right) + 13.66\left(\frac{a}{W}\right)^2 - 23.98\left(\frac{a}{W}\right)^3 + 25.22\left(\frac{a}{W}\right)^4$	P, applied load (N) l, specimen length (m) B, specimen thickness (m) W, specimen height (m) a, crack length (m) Y, dimensionless constant
Single-edge cracked tension or compact tension	$K_I = Y\frac{P\sqrt{a}}{BW}$ $Y = 1.99 - 0.41\left(\frac{a}{W}\right) + 18.70\left(\frac{a}{W}\right)^2 - 38.48\left(\frac{a}{W}\right)^3 + 53.85\left(\frac{a}{W}\right)^4$	
Double cantilever beam	$K_I = 3.45\frac{Pa}{Bh^{3/2}}\left[1.0 + 0.7\left(\frac{h}{a}\right)\right]$	$2h$, specimen height (m)
Double torsion	$K_I = PW_m\left[\frac{3(1+\nu)}{Wd^3 d_n}\right]^{1/2}$	d_n, thickness of the groove (m) W_m, moment arm

Source: Adapted from Ref 54

gested that under certain limitations the applied load, together with the scratched area, can be a convenient means to predict the adhesion of thin coatings. Sekler et al. (Ref 60) discussed techniques to determine the critical load.

The scratch test has been applied in the evaluation of thermally sprayed coatings (Ref 62-66), although there may be a technical difficulty because the theories developed for thin coatings may no longer be appropriate for bulk coatings. Das et al. (Ref 62), in studying plasma-sprayed yttria-stabilized zirconia (YSZ) coatings, proposed a method for determining the critical load and discussed the effect of loading rate (dL/dt) and the scratch table speed (dx/dt). It was found that the critical load is independent of loading rate and scratch speed because there were no significant strain-hardening effects of YSZ during the scratch tests. However, when the tests were performed at a very high scratch speed (≥15 mm/min) or loading rate (>200 N/min),

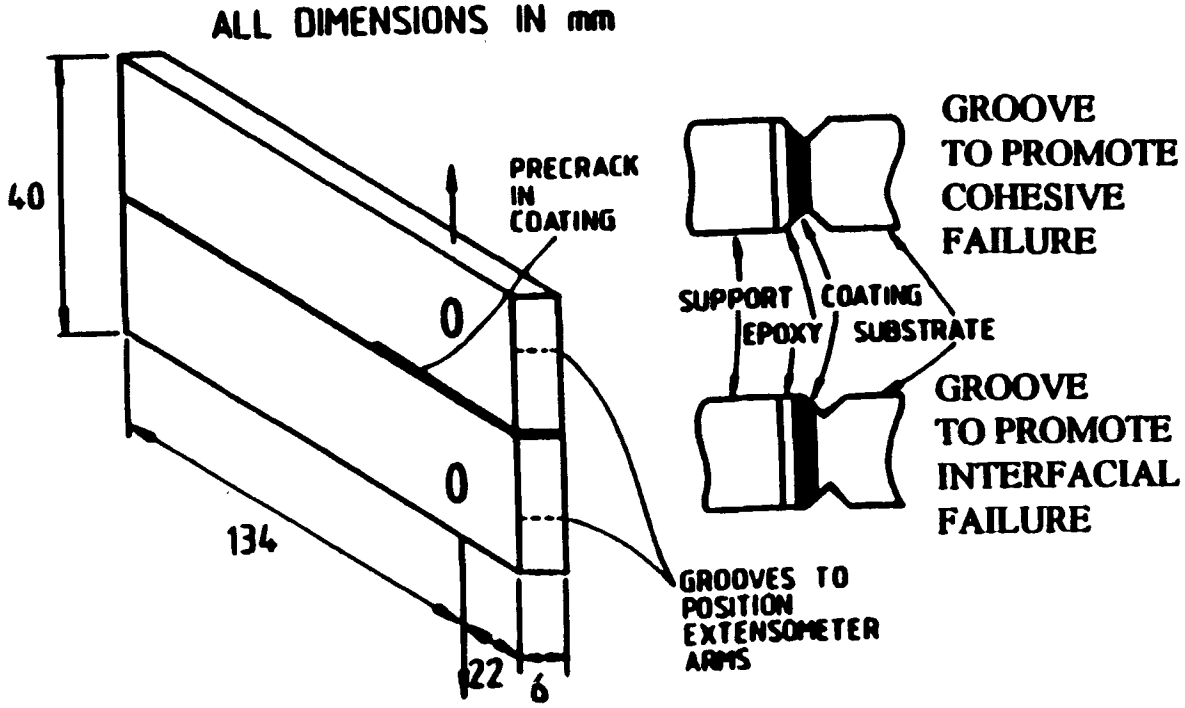

Fig. 17 DCB specimens used for adhesion measurement. Detail shows the grooving procedure to promote either interfacial or cohesive failure

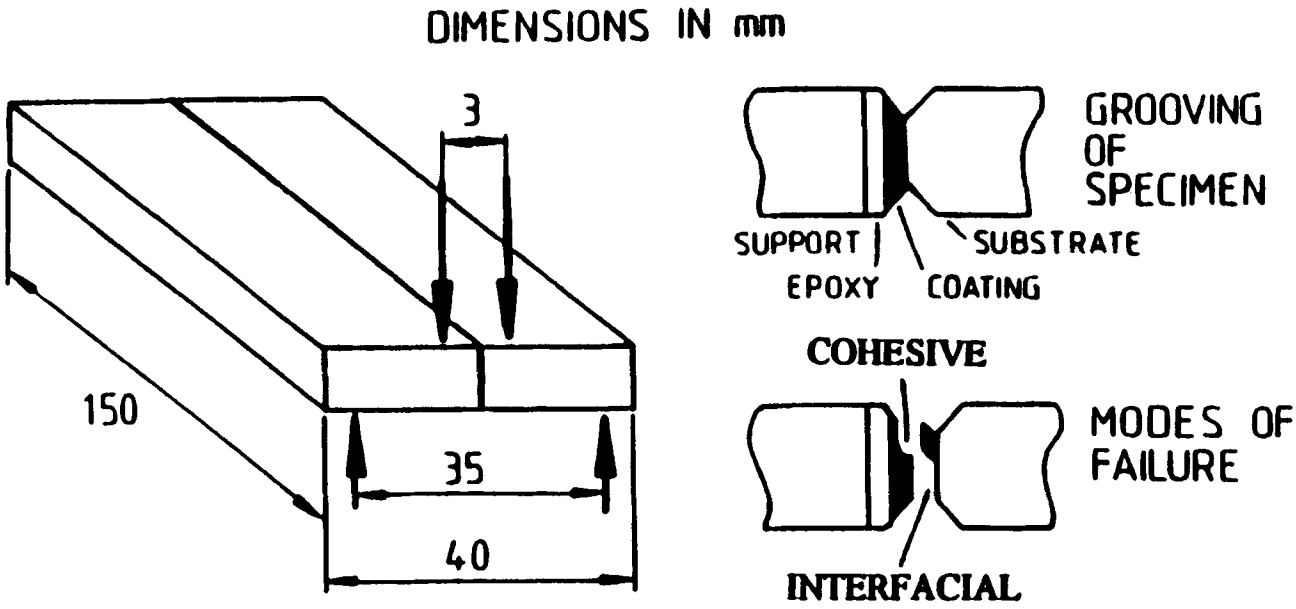

Fig. 18 Double torsion geometry and test configuration. Detail shows grooving of specimen and modes of failure

determination of critical load became difficult. Scratch tests have been performed on the cross section of alumina-based coatings (Ref 65, 66). A half-cone-shaped fracture was formed as the indenter approached the free surface (Fig. 21). The height of this cone can be related to the cohesion strength or intrinsic fracture toughness of the coating. Interfacial cracking may also occur and can be used as a measure of adhesion strength. The fracture toughnesses of some alumina composite coatings and sintered alumina are listed in Table 6.

2.4 *Acoustic Emission*

2.4.1 Background

Acoustic emission (AE) describes "a class of phenomena whereby transient elastic waves are generated by the rapid release of energy from localized sources within a material" (Ref 67). The energy usually arises from one or a combination of sources (Ref 68), including phase transformation, plastic deformation, corrosion, and crack initiation and growth (Ref 69). An AE event is detected by a piezoelectric transducer when energy is released from the material. The output is amplified and then features of the AE signal, such as the ring down count, rise time, and/or pulse height, are analyzed (Fig. 22). A multichannel system often is used to examine different energy levels; the signal may also be digitized or integrated for an energy analysis.

Special interest lies in formulating crack initiation and growth criteria based on the microstructural design of coatings. This is important because microstructural features can be quantitatively determined (Ref 70) by image analysis methods and the microstructure of coatings can be "controlled" by the thermal spray process. Acoustic emission technology has been combined with fracture mechanics measurements (Ref 52, 62, 71) or thermal tests (Ref 72, 73) to characterize coating properties and has been applied to better understand failure mechanisms and to predict lifetimes (Ref 74-76). It has also been applied to quality control and in-service monitoring.

2.4.2 Crack Density Function

A thermal spray coating has a very rich microstructure, and both macro- and microcracking, among other sources, can release energy during coating service. A difficulty is that the AE response is overwhelming with regards to acquiring data and this often limits the AE method to be a qualitative technique, because individual AE response-to-coating morphology correlations cannot be made. However, quantitative AE analysis may still be possible through a test procedure that includes calibration (Ref 77, 78). For example, studies on thermal barrier coatings that were subjected to heat cycling changed from a systematic response to a stochastic response upon a certain thermal cycle. This was considered to be indicative of a change from micro- to macrocracking, because the change in AE response corresponded to the observation of the formation of large cracks (Fig. 23) (Ref 79).

The record of AE response for coatings will be a combination of all possible noise origins and a "crack density function" (CDF) (Ref. 77, 80) which incorporates both the number and size of cracks has been proposed. It is found that microcracking events tend to occur at low values of CDF. Figure 24 shows an example of a CDF analysis for two coatings that were prepared

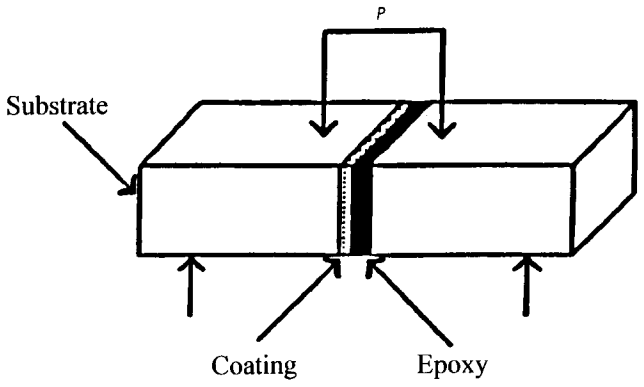

Fig. 19 Four-point bending specimen. The coating was attached by epoxy to the other support bar. Source: Ref 51

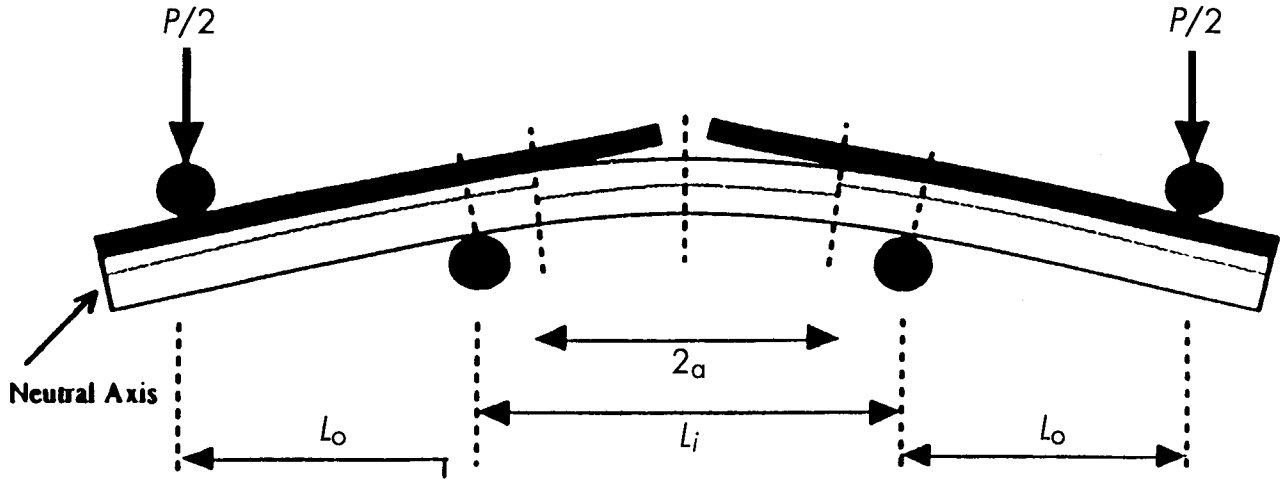

Fig. 20 Loading arrangement and specimen geometry to measure coating adhesion. The coating was precracked to the interface between the coating and the substrate. Source: Ref 53

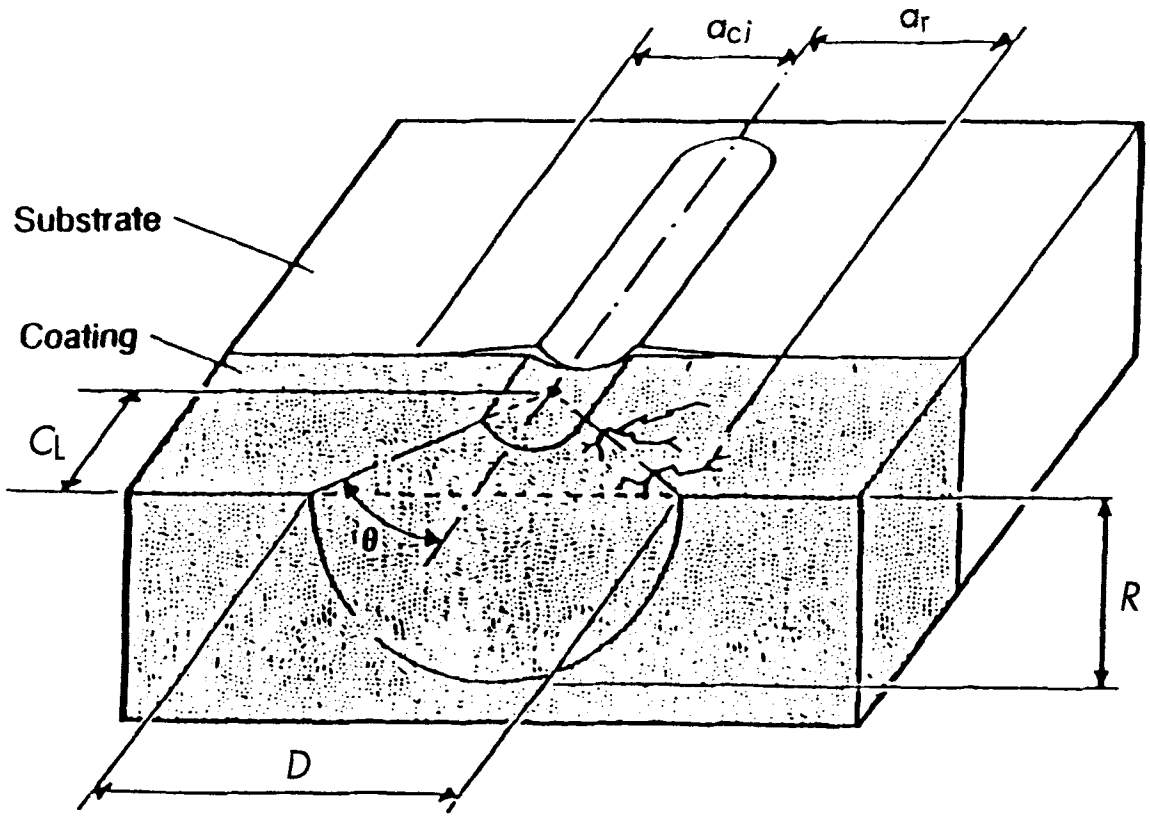

Fig. 21 Schematic of the damage produced during a scratch adhesion/cohesion test. Source: Ref 66

Table 6 Fracture toughness of various alumina composite coatings and sintered alumina

Material(a)	K_c, MN · m$^{-3/2}$
Al_2O_3 (sintered)	4.8
Al_2O_3	2.7
Al_2O_3-3TiO_2	2.1
Al_2O_3-13TiO_2	2.4
Al_2O_3-40TiO_2	2.2
Al_2O_3-13TiO_2 (flame sprayed)	1.4
Al_2O_3-30MgO	2.7
Al_2O_3-20ZrO_2	2.9
Al_2O_3-40ZrO_2	3.0

(a) All the materials, except for the first, are thermal spray coatings. Source: Ref 66

so as to exhibit different behaviors. The essential details are that one sample (indicated by the solid portions of the histogram) exhibited a lower frequency of the CDF function, which is indicative of a lower degree of cracking, both in terms of the number of cracks and crack size (since the CDF incorporates these physical characteristics of coatings). The frequency of these events increased at failure and after failure (Fig. 24b and c).

Acoustic emission methods have also been used in conjunction with mechanical property measurements. For instance, it has been established that the number of AE counts emitted during a hardness test increased as the density of the material decreased. Figure 25 indicates a number of processes and materials where it is generally understood that flame spraying (indicated by "f") will produce a less dense deposit than plasma spraying ("p") and that additions of titania to alumina will increase the deposit density. Thus, an intuitive interpretation is that the most dense material exhibits the least cracking behavior (at least under the constant force conditions of a hardness test), and this is reflected in a lower AE response.

Similar correlations have been proposed on the basis of AE measurements performed during TATs. The AE count accumulated during a TAT is plotted with respect to the so-determined bond strength in Fig. 26. The coatings that incorporate metallic constituents exhibit a lower activity than the nonmetallic coatings (at equivalent bond strengths). Therefore, a physical interpretation of the mechanical response is that the metallic materials allow more plastic deformation than the ceramic materials. This simple explanation relates well to the general understanding of bulk material behavior; that is, ceramics are more brittle than metals. However, one caution is that such correlations between bulk material properties and thermally sprayed materials may be incorrect, because these thick coatings are formed by a rapid solidification process.

The point of this discussion is that adhesion and cracking mechanisms are symbiotic material properties that can be linked by AE processes. Thus, in a very broad sense, the study and understanding of cracking mechanisms will lead to real improvements in maximizing the adhesion of coatings. For example, consider relating the AE response during a TAT to the cracking

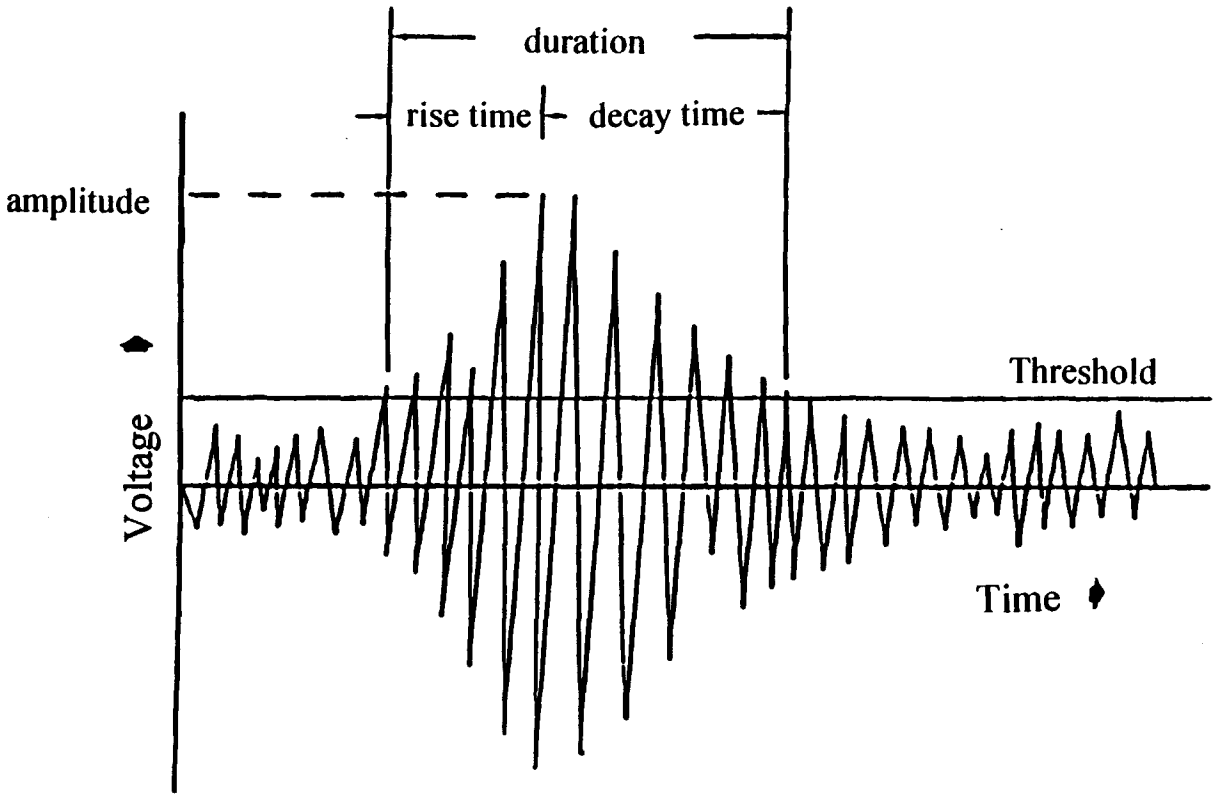

Fig. 22 Typical transducer output accompanying burst emission

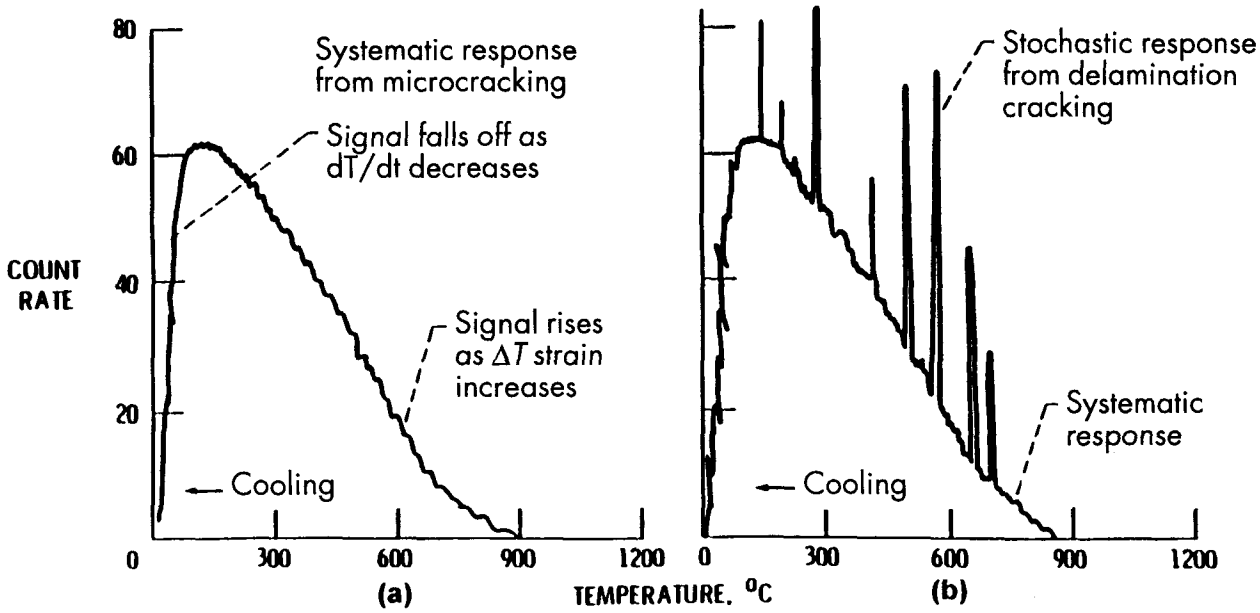

Fig. 23 Schematic of AE effects. (a) Typical cooling cycle. (b) Failure during cooling cycle. Source: Ref 79

and deformation behavior of the specimen assembly. Figure 27 shows that the strain in the bond coat (the metallic constituent) is always greater than the ceramic strain, although the absolute extension in the ceramic layer is greater than that of the bond coat. The overall conclusion is that cohesive failure occurs by many microcracks throughout the material, whereas interfacial failure has a lower density of cracks. Another implication is that cracking during a TAT always begins at the edges of the material and

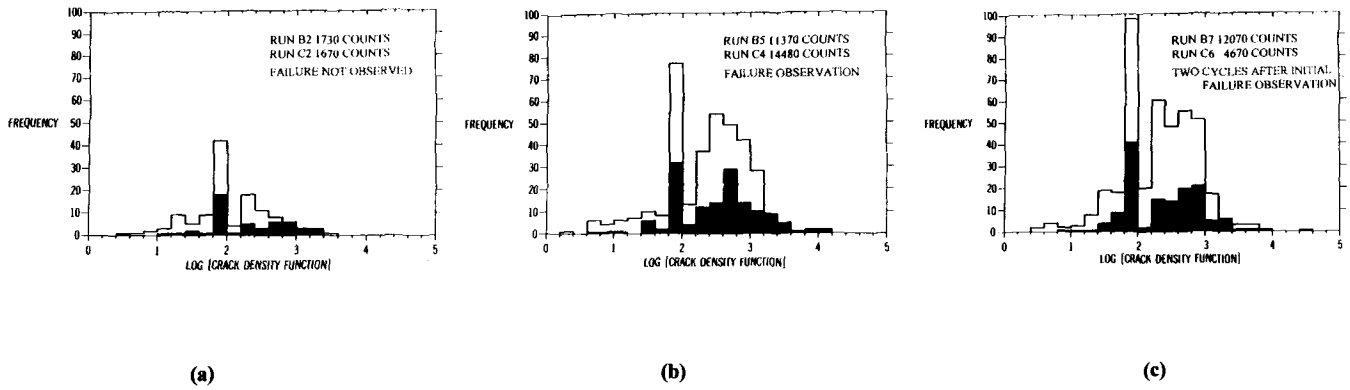

Fig. 24 Crack density function analysis of coatings. (a) First thermal cycle. (b) Failure cycle. (c) Two cycles after failure

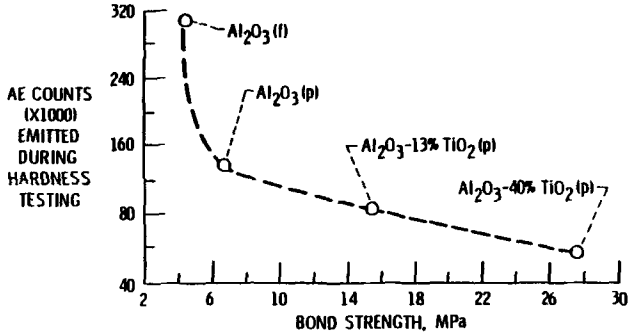

Fig. 25 Bond strength versus AE counts emitted during hardness testing. f, flame sprayed; p, plasma sprayed

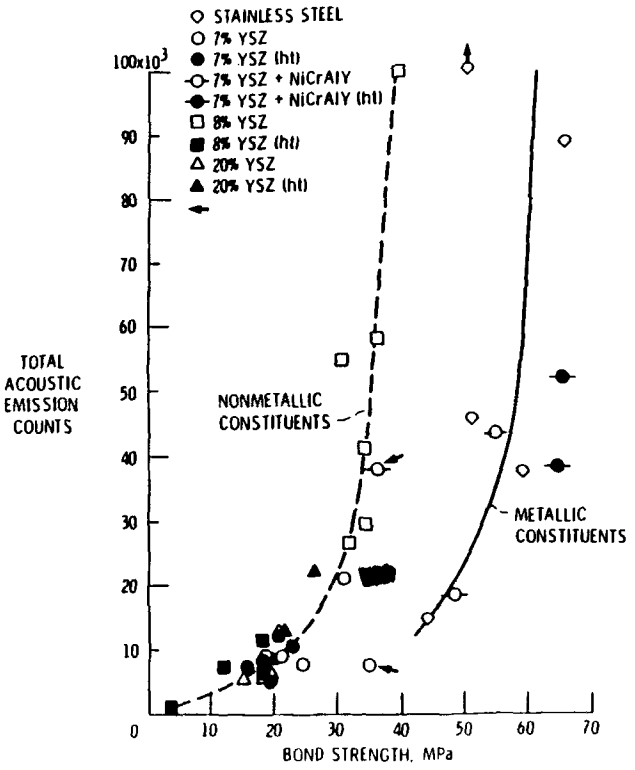

Fig. 26 Bond strength versus AE counts emitted during tensile testing. ht, heat treated

that flaws in this region, being the weakest link, may dictate the so-determined strength value.

2.5 *Other Test Methods*

2.5.1 Ultrasonic Test

Ultrasonic testing is a potential nondestructive method for evaluating the adhesion strength of coatings (Ref 81). Ultrasonic waves are generated by a transmitter, and then the reflected or transmitted waves can be received (Fig. 28). Early studies (Ref 82) revealed that the backwall echo disappeared completely in a region of poor adhesion, such as in the presence of pores or air interfaces where the incident wave and reflected waves cannot be transmitted. Francke and de Gee (Ref 83) used higher frequencies of 5 to 10 MHz to assess such interface effects and suggested that the transmission method was more promising, even though the backwall method was feasible. Other workers (Ref 84) examined plasma-sprayed aluminum and found that the attenuation of sound waves was sensitive to coating thickness. More recent studies (Ref 85) examined TATs by ultrasonic methods and found that the bottom echo height, B_c, had a tendency to increase with increasing adhesion strength (Fig. 29). The effect of spraying condition on the bottom echo (Fig. 30) indicated a stronger backwall echo for coatings prepared under optimal spray conditions.

2.5.2 Some Tests Not Covered

Many other methods are used to evaluate adhesion qualitatively or quantitatively. Examples include:

- Wear tests (Ref 86, 87), which are related to the interfacial or cohesive strength of coatings
- Thermal tests (Ref 88, 89) during thermal cycling and thermal shock protocols that influence adhesion strength during heating and cooling processes

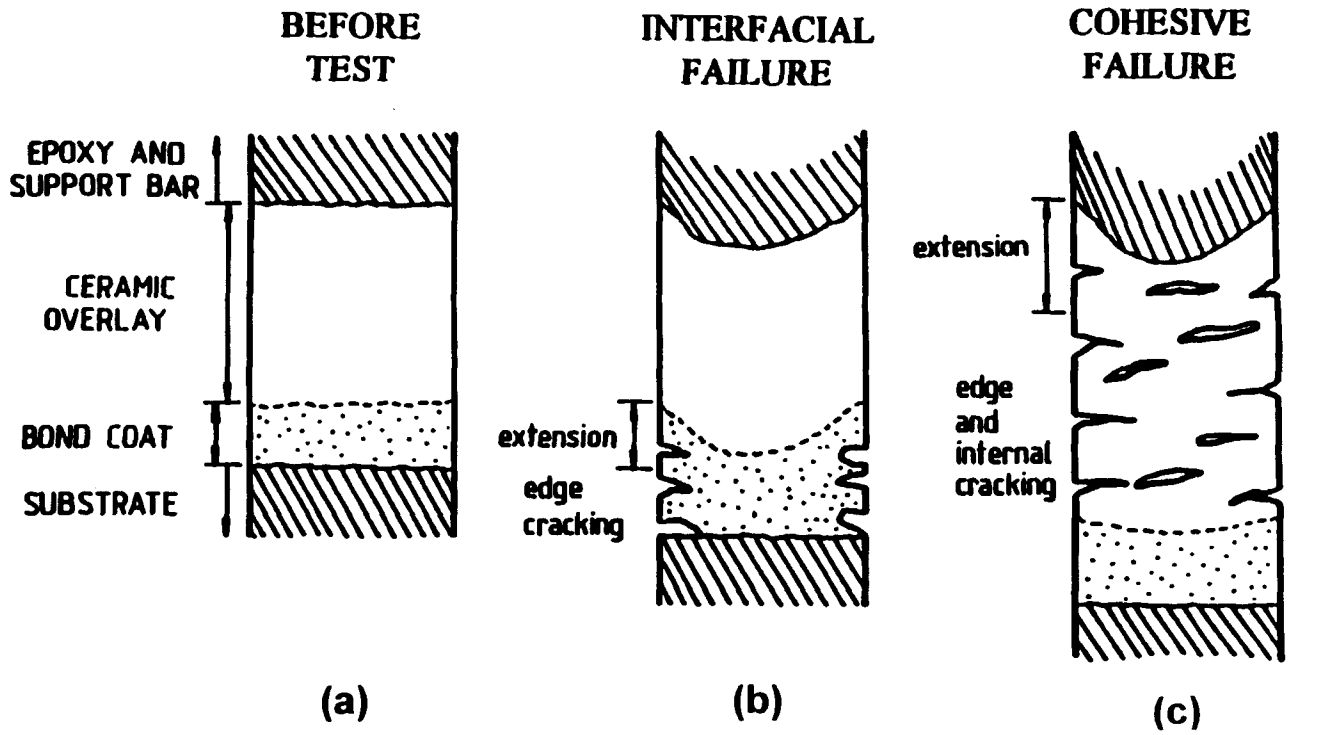

Fig. 27 Schematic illustrating the coating deformation response during the interfacial and cohesive failure modes. (a) Original specimen setup. (b) Interfacial failure mode. (c) Cohesive failure mode

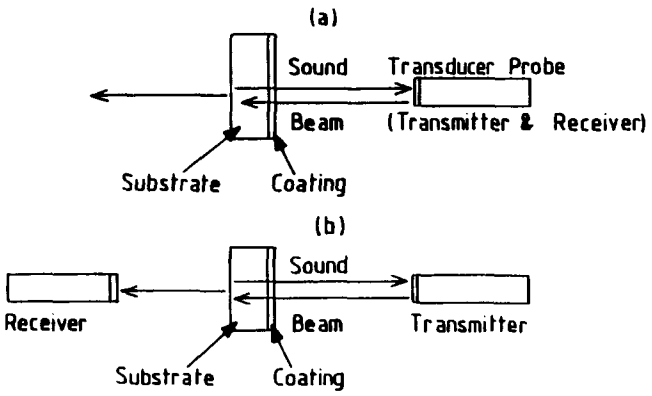

Fig. 28 Schematic diagrams of (a) backwall reflection and (b) transmission methods of ultrasonic testing

- Shear tests (Ref 90, 91) which may best reflect in-service conditions
- Modified short bar (Ref 92) and crack-opening displacement methods (Ref 93) for measuring fracture toughness
- Peel tests (Ref 94, 95), which may be a potential candidate for adhesion testing of thermal sprayed polymer coatings

There is still no ideal adhesion test that can satisfy all requirements. Modification of existing techniques and design of new methods may offer further improvement.

3. Indentation Assessment of Thermal Spray Coatings

The methods discussed above provide many different approaches to evaluate the adhesion or cohesion strength of coating systems. However, each has disadvantages and none can elucidate the differences of in-service performance. For example, TATs suffer from epoxy penetration and alignment problems. The DCB method requires elaborate and expensive test equipment and special specimen preparation. On the other hand, the indentation technique, which has been used successfully to measure the fracture toughness of a wide range of bulk materials, is a single test that can be used to assess the fracture toughness of sprayed coatings. The microhardness distribution within the coatings, which reflects variations in the coating system, may provide evidence of the influence of operation conditions on thermal spray coatings.

3.1 *Indenters and Cracking Systems*

Indentation techniques are often used as surface characterization tests. The hardness of a material implies its resistance to permanent indentation. Indentation tests are classified as either sharp or blunt. Specific crack patterns can be observed in the material at certain loads on the indenter (Ref 96).

3.1.1 Blunt Indenter

Contact between the indenter and the material is predominantly elastic prior to fracture and can be regarded as blunt. This concept was examined by Hertz (Ref 97), who, motivated by the

question of the physical significance of hardness, analyzed the physics of contact between two curved bodies. A qualitative description of the cone-shaped crack that runs around the contact circle and spreads downward into the bodies at critical loading (Fig. 31) was formulated. This so-called Hertzian cone crack is usually generated by a relatively hard spherical indenter; Fig. 31 shows schematically the sequence of events for a complete loading/unloading cycle (Ref 98).

3.1.2 Sharp Indenter

Sharp indenter conditions apply when the contact is essentially plastic in nature and implies irreversible deformation. The sharp indenter is favored because it is a convenient way to measure not only hardness but also fracture toughness. Figure 32 illustrates the sequence of events for a complete indentation cycle where median, radial, and lateral crack systems are formed (Ref 96, 98).

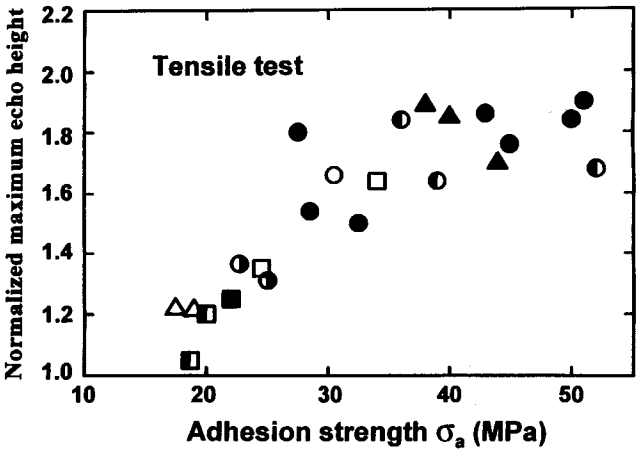

Fig. 29 Relationship between adhesion strength measured by tensile testing and evaluation of results by ultrasonic testing. The symbols represent the various thermal spray parameters that were used during preparation of the coatings. Source: Ref 85

3.2 *Fracture Toughness Measurement*

3.2.1 Indentation Fracture Toughness

Thermal spray coatings have a distinctive layered microstructure that is heterogeneous, and thus cracking mechanisms are different for the indentation in the cross section and in-plane orientations. When indentation is performed in the cross section, the coatings tend to crack along the lamella interface (along the in-plane indentation direction) as well as from the four corners of the indenter (Fig. 33)(Ref 99). Although thermal spray coatings do not behave ideally under indentation, this technique has been used to assess the fracture toughness of coatings (Ref 100-102).

3.2.2 Interface Fracture Toughness

Adhesion strength was studied by Dal Maschio et al. (Ref 102) using a fracture mechanics approach via indentation along the coating/substrate interface. A set of Vickers indentations, using 50 and 100 N, were made at the ceramic/bonding interface (Fig. 34). The crack length was measured by optical and/or electron microscopy, and the critical energy release rate was considered as a function of substrate temperature during the spray coating process. Table 7 compares the results of several workers. The indentation fracture toughness measurements tend to be greater than those obtained from DCB tests. Aspects of these measurements have led to critical discussion, based primarily on the application of the indentation theory to highly anisotropic thermal spray coatings. Obtaining a symmetrical crack pattern during any test is never ensured, because the coating microstructure has many features that influence crack formation and propa-

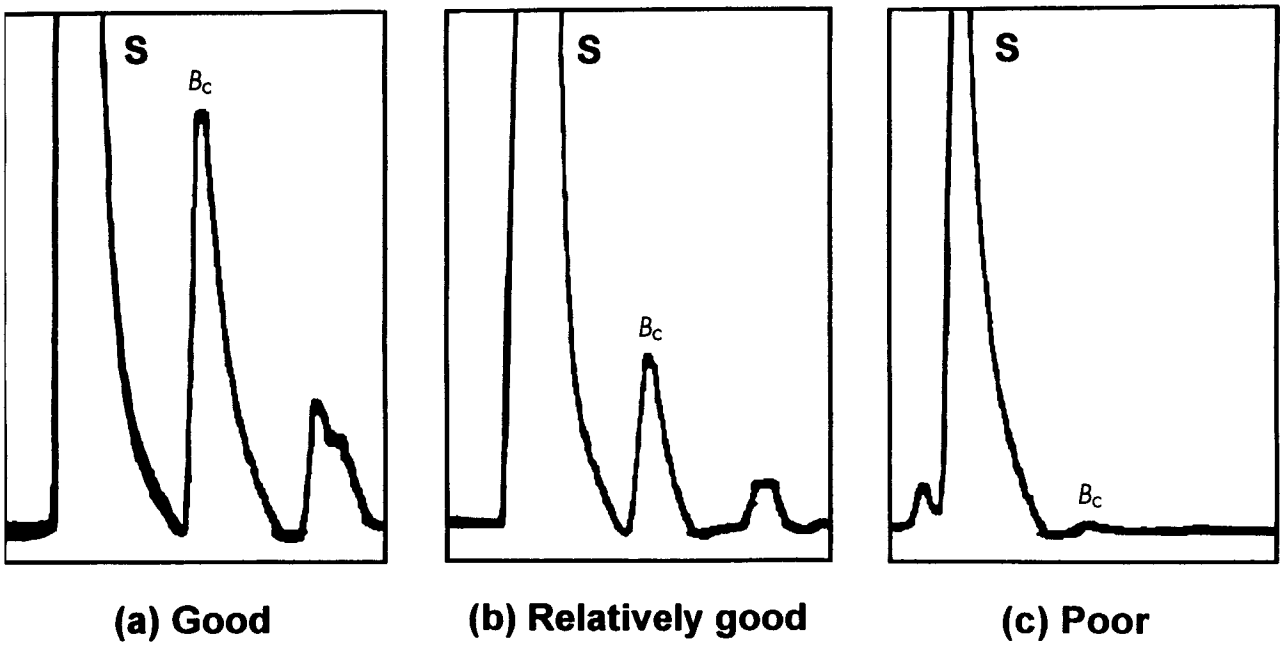

Fig. 30 Effect of spray condition on bottom echo height, B_c, during ultrasonic testing. Source: Ref 85

gation; therefore, the so-determined values are often highly variable. For example, the Weibull modulus of an alumina coating is 0.5 and the modulus of an alumina-titania coating is 0.8 (Ref 99). The other main point, as will be discussed in the following section, is that coatings are highly anisotropic throughout their thickness; consequently, randomly placed indentation

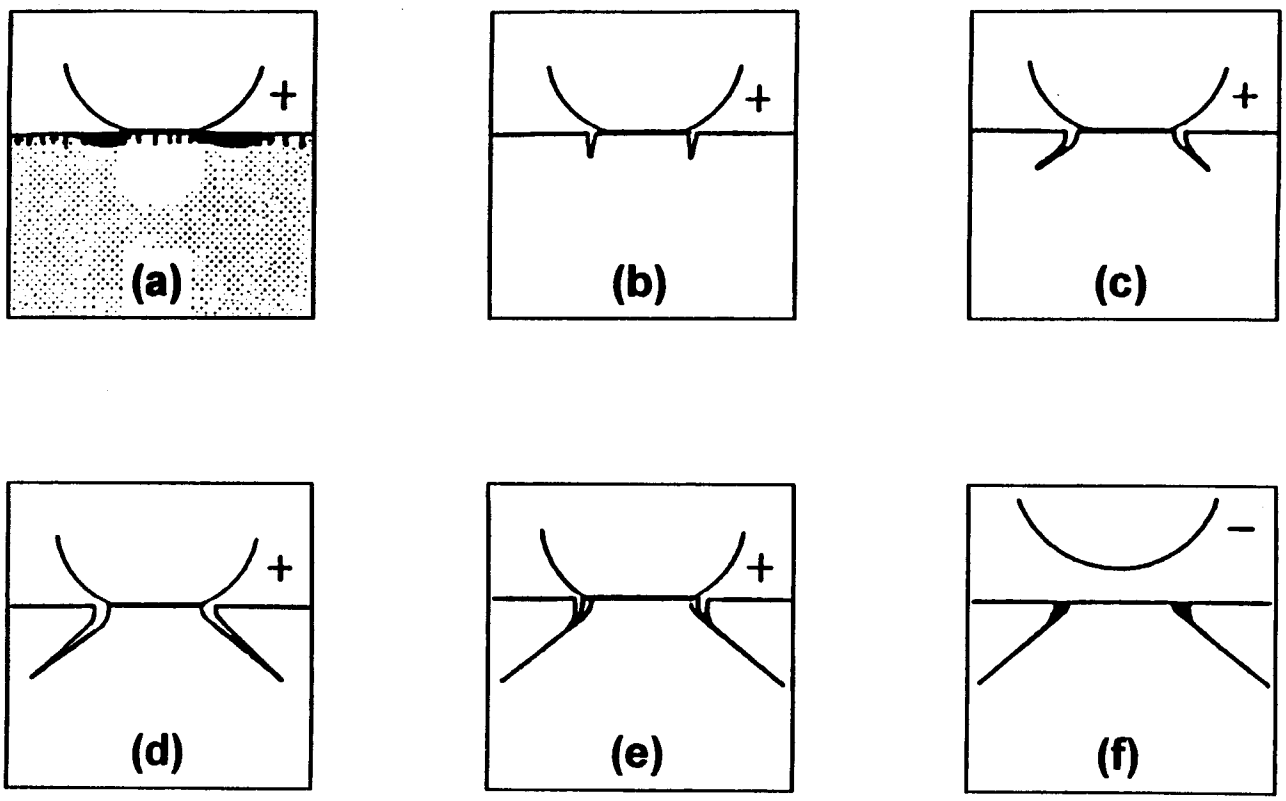

Fig. 31 Evolution of a Hertzian cone crack during blunt indenter loading (+) and unloading (–). The tensile (black) and compressive (unshaded) stress fields are shown in (a). Source: Ref 98

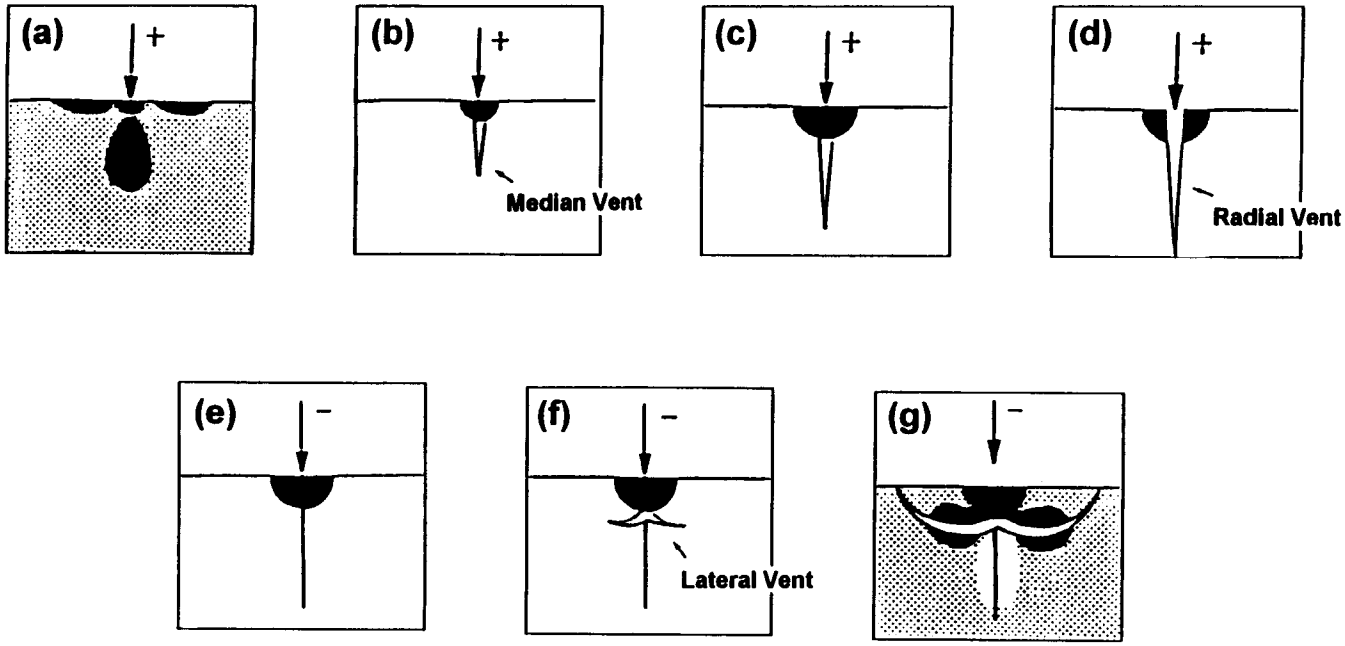

Fig. 32 Evolution of median, radial, and lateral crack systems during sharp indenter loading (+) and unloading (–). The black region in each drawing indicates the plastic zone. Point loading and residual stress field s are shown in (a) and (g), respectively. The black and unshaded regions represent tensile and compressive stress fields, respectively. Source: Ref 99

fracture mechanics tests would not be expected to produce consistent values.

3.3 *Anisotropy Assessment of Thermal Spray Coatings*

3.3.1 Microhardness and Anisotropy of Thermal Spray Coatings

The microstructure of thermally sprayed coatings is a mix of lamellae, pores of varying geometry, and oxides. It is recognized that such coatings are not homogeneous, and microhardness measurements can be used to examine any anisotropy. The mean values of microhardness and the distributions of data sets across the coating thickness change with respect to test position (Ref 103). Hence, characterizing thermally sprayed coatings only in terms of their hardness is of limited value, because hardness depends on the precise location of the measurement. However, microhardness measurements can quantify the material property variation in the specimen if the Weibull modulus is determined. In this fashion it was found that, at least for the data presented by Berndt et al. (Ref 103), the variability of surface properties is greater compared to the properties throughout the specimen cross section. The morphology of microhardness indents also changes, and this feature can be used to study variations in homogeneity and stress concentration within the specimen.

As shown in Fig. 35, the Weibull modulus fluctuates and suggests that the data distributions are a reflection of microstructural changes in the bond coat. For example, the variation in m may imply the formation and distribution of oxides and crack networks. Weibull distributions will be addressed in greater detail later in this paper.

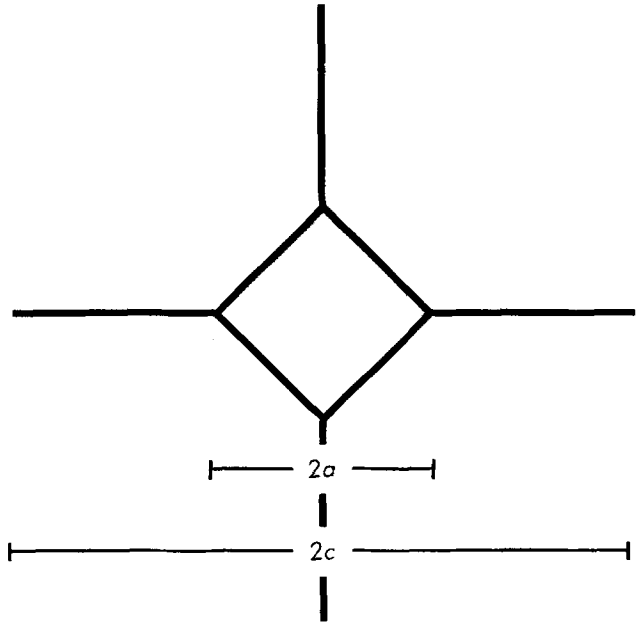

Fig. 33 Schematic of a Vickers indentation showing characteristic dimensions of crack length, c (i.e., the median crack length), and hardness impression, a

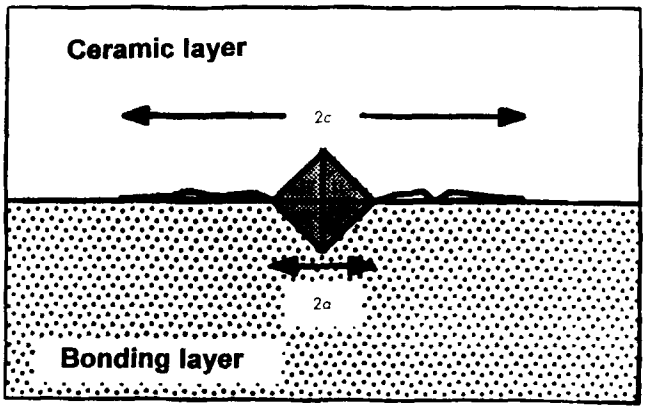

Fig. 34 Schematic of interfacial Vickers indentation. Source: Ref 102

3.3.2 Interpretation to Lifetime

Microhardness measurements have been used to monitor coating behavior after thermal treatments (Ref 104). For example, a series of thermal barrier coatings (a NiCoCrAlY intermetallic bond coat and cerium-stabilized zirconia layer) aged at different times and temperatures (at 400 and 800 °C for 100, 500, and 1000 h) were tested for microhardness to assess any material property changes (Ref 105). The major failure mechanisms of thermal barrier coatings are oxidation within the bond coat and cracking due to thermal expansion mismatch within the coating system (Ref 106). This can be reflected by the hardness variation, and, in the future, a failure model and lifetime prediction may be based on analysis of such data.

Temperature effects, such as heat treatment, thermal shock, and thermal cycle, were observed in the coating systems. For ceramic coatings, microcracks produced by thermal expansion mismatch may have different size and density. These cracks will be responsible for variations in mechanical properties. At the same time, the oxide film surrounding the lamellae within the bond coat should have different thicknesses according to the oxidation kinetics at various temperatures. These oxide films, although they may contribute to the increase of microhardness, decrease the adhesion strength of the bond coat. Schematic illustrations of mechanisms that cause coating variations are presented in Fig. 36. Nonmonotonic response of hardness and the low Weibull modulus imply complex processes such as stress re-

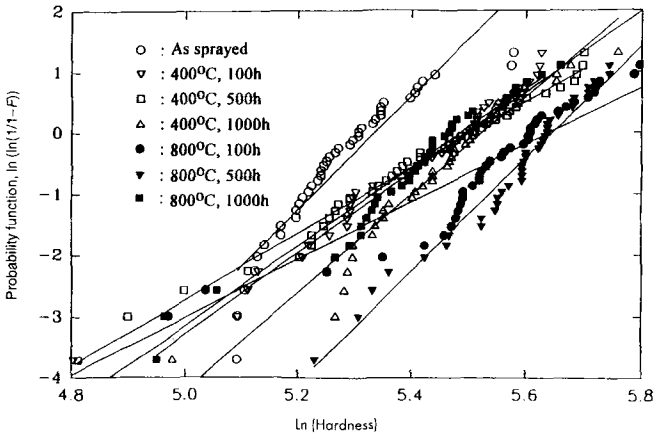

Fig. 35 Weibull plots of microhardness data for as-sprayed and aged samples within a bond coat

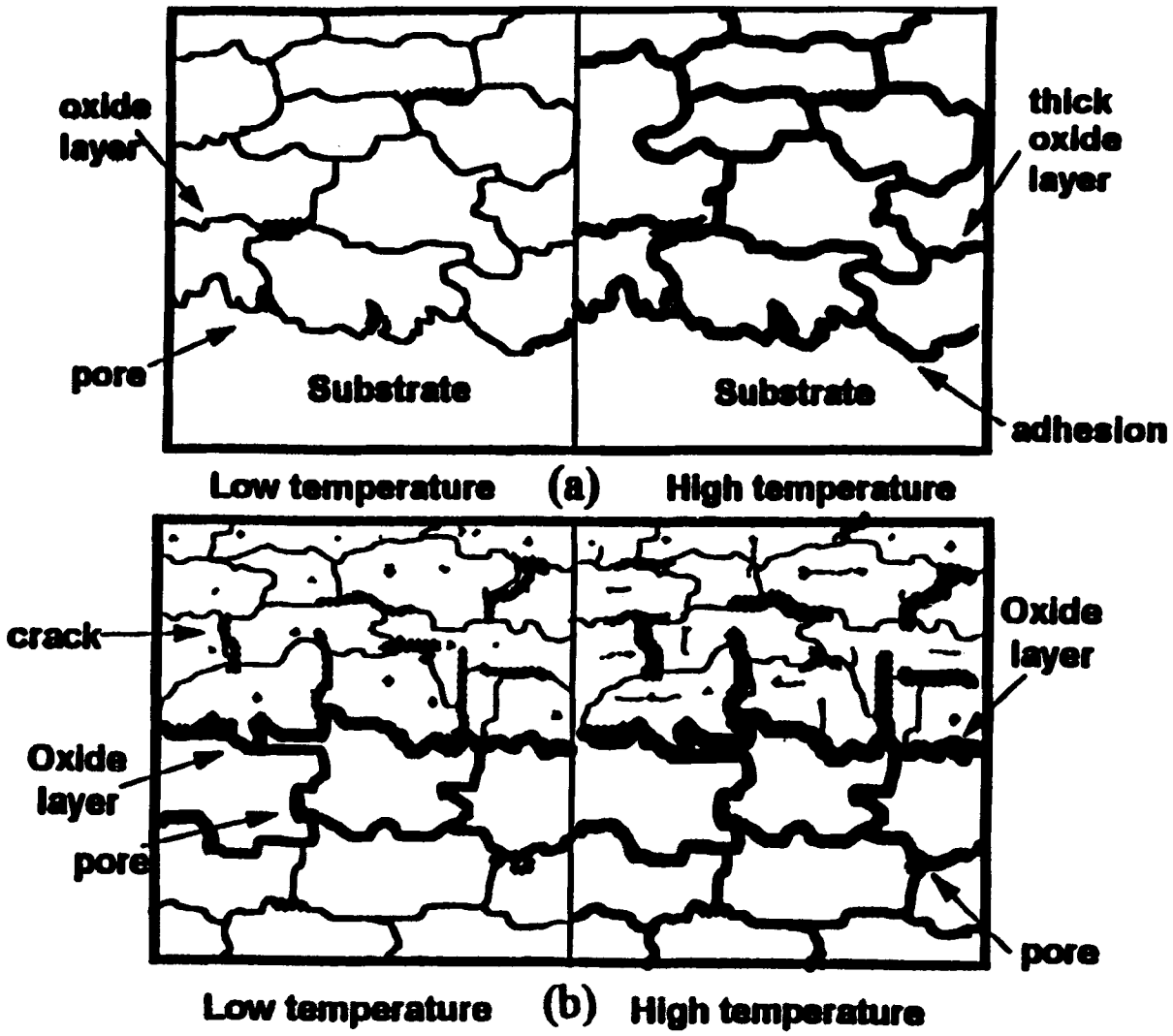

Fig. 36 Physical models of (a) bond coat/substrate interface and (b) bond coat/ceramic coating interface at low and high temperatures

Table 7 Fracture toughness by indentation technique

Material	Mean K_{IC}, N · m$^{-3/2}$	Standard deviation	Load, N	Ref
Al_2O_3	209	...	47	23
	189	...	98	23
	97.6	...	147	23
Al_2O_3-2.5TiO_2	218	...	73.5	23
	268	...	147	23
	301	...	98	23
YSZ	24.0	6.4	588	100
Cr_2O_3	43.0	5.2	9.8-98	101
Spinel	47.0	12.7	294	100
(12Si-Al)-(ZrO_2-8Y_2O_3)(a)	11.1	1.3	50	102
	10.4	1.3	100	102
(12Si-Al)-(ZrO_2-8Y_2O_3)(b)	16.0	1.0	50	102
	21.2	1.2	100	102
(12Si-Al)-(ZrO_2-8Y_2O_3)(c)	5.7	0.9	50	102
	3.8	0.5	100	102
(12Si-Al)-(ZrO_2-8Y_2O_3)(d)	5.3	0.5	50	102
	5.8	0.7	100	102

(a) to (d) Interfacial fracture toughness for four different spraying conditions adapted from Ref 102

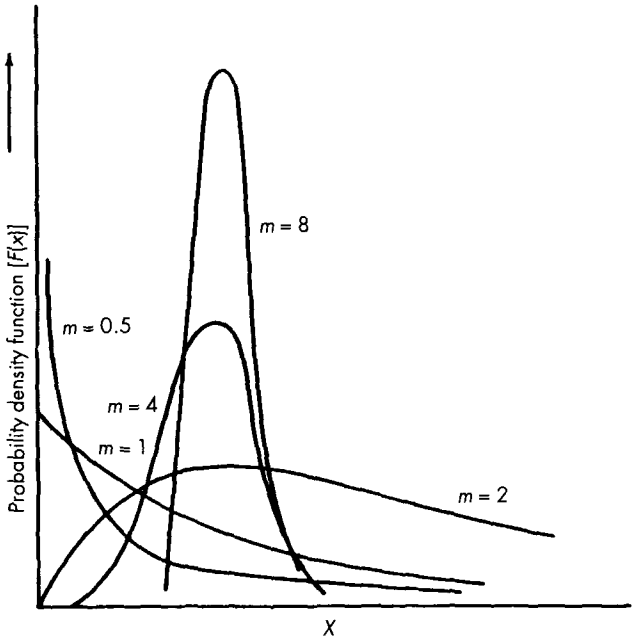

Fig. 37 Probability density function of a Weibull distribution for different values of Weibull modulus, m. The horizontal axis (x) represents experimental data, such as microhardness. Source: Ref 110

laxation, growth of oxides within the bond coat, and phase changes.

Thermal cycling of thermal barrier coatings not only deteriorates the strength of the material at and near the bond coat interface but also reduces the reliability of the ceramic thermal barrier layer. Microhardness measurements can be used to quantify the material property variation in the specimen. Weibull modulus values obtained in the study (Ref 104) show that the reliability of the ceramic coating decreases from 10.5 before cycling to 5.5 after thermal cycling. The wide scatter in the hardness data indicates the variable nature of stress concentration at the test location.

Thus, increasing the reliability of coatings by controlling the variable nature of the material properties requires that the mechanical response throughout coatings be precisely quantified. Microhardness has been selected because this property has been used by many authors not only to characterize specific coatings but also to compare coatings formed from different feedstock materials, spray processes and process parameters.

4. Statistical Analysis

4.1 *Weakest Link Theory*

Brittle materials usually contain a certain number of flaws. Weibull (Ref 107) assumed that a stressed brittle material can fail due to any of a number of independent flaws, each containing an infinitesimal probability of failure, $(\Delta P_f)_i$. The probability that the ith flaw will not cause failure is $(P_s)_i = 1 - (\Delta P_f)_i$. The overall probability of survival, P_s, defined as the reliability function, is the product of the individual probabilities of survival, that is (Ref 108):

$$P_s = \prod_i (P_s)_i = \prod_i \left\{1 - (\Delta P_f)_i\right\} \quad \text{(Eq 7)}$$

$$P_s \cong \prod_i \exp\left\{-(\Delta P_f)_i\right\} \quad \text{(Eq 8)}$$

$$P_s = \exp\left\{-\sum_i (\Delta P_f)_i\right\} = \exp\left\{-\Phi(x)\right\} \quad \text{(Eq 9)}$$

The function $\Phi(x)$ was called the "risk of failure" by Weibull. The only necessary general condition that $\Phi(x)$ must satisfy is to be a positive, nondecreasing function, vanishing at a threshold value x_u, which does not need to be zero. Weibull found that the most simple function satisfying this condition is

$$\Phi(x) = \left(\frac{x - x_u}{x_o}\right)^m \quad \text{(Eq 10)}$$

Thus,

$$P_s = \exp\left\{-\left(\frac{x - x_u}{x_o}\right)^m\right\} \quad \text{(Eq 11)}$$

The Weibull function, or the failure probability function for a random variable x, is given as:

$$F(x) = 1 - \exp\left[-\left(\frac{x - x_u}{x_o}\right)^m\right] \quad \text{(Eq 12)}$$

where m is the Weibull modulus (or shape factor), which reflects the data scattering within the distribution; x_o is a characteristic value (or scale factor), below which 63.2% of the data lie; and x_u is a threshold value (or location factor). Thermal spray coatings that possess defects such as porosity and cracks are subject to the weakest link theory, because these areas have the highest probability of failure.

4.2 *Characteristics of the Weibull Distribution*

The Weibull distribution has been used to describe a wide range of problems and is a popular method for life-testing applications (Ref 109, 110). Usually, x_u can be set to zero (Ref 110), because this ensures the minimum probability. Then the two-parameter Weibull distribution is

$$F(x) = 1 - \exp\left\{-\left(\frac{x}{x_o}\right)^m\right\}, \quad x \geq 0 \quad \text{(Eq 13)}$$

The remainder of this discussion will focus on the two-parameter Weibull function.

The Weibull distribution is different from the normal Gaussian distribution, because it can be skewed with respect to m and

x_0 (Fig. 37) (Ref 110). The mean value, μ, and variance, σ^2, are defined as:

$$\mu = \int_0^\infty x f(x) dx \quad \text{(Eq 14)}$$

$$\sigma^2 = \int_0^\infty (x - \mu)^2 f(x) dx \quad \text{(Eq 15)}$$

where $f(x)$ is the corresponding probability density function of the Weibull distribution. After integration:

$$\mu = x_0 \Gamma\left(\frac{1}{m} + 1\right) \quad \text{(Eq 16)}$$

$$\sigma^2 = x_0^2 \left[\Gamma\left(\frac{2}{m} + 1\right) - \left\{\Gamma\left(\frac{1}{m} + 1\right)\right\}^2\right] \quad \text{(Eq 17)}$$

where Γ is the gamma function. The gamma function approaches unity for values of 1. Therefore, examination of Eq 16 and 17 indicates that as the Weibull modulus, m, increases, the mean, μ, approaches the characteristic value x_0 and the variance, σ^2, approaches zero (Table 8). The volume of the specimen should be considered if numerous flaws are inside the specimen. Davies (Ref 111) discussed the size effect of the test specimen and established the following relationship:

$$\frac{\mu_1}{\mu_2} = \left(\frac{V_{E2}}{V_{E1}}\right)^{1/m} \quad \text{(Eq 18)}$$

where μ is the mean value, V_E is the volume, and the subscripts 1 and 2 represent two different specimens.

4.3 *Estimation of Weibull Parameters*

There are many ways to obtain Weibull parameters from experimental data, such as Weibull plots, the maximum likelihood method, linear estimators, and nonlinear direct curve fitting. However, such analyses can be complicated, and no single method is satisfactory for all circumstances. One simple procedure is to plot the experimental data and then determine, by the appearance of the graph, whether the Weibull function is applicable.

4.3.1 Weibull Plots

Weibull plots are the most common means for obtaining Weibull parameters. The plots are ascertained by rearranging Eq 13 and taking natural logarithms twice. Thus, x_0 and m can be determined by curve fitting the following:

$$\ln\left[\ln\left(\frac{1}{1 - F(x)}\right)\right] = m(\ln x - \ln x_0) \quad \text{(Eq 19)}$$

The value of $F(x)$ in Eq 19 has been discussed in Ref 110 and 112. The mean value of $F(x)$ is obtained from placing the data in ascending order and letting

Table 8 Mean and variance of Weibull distribution as a function of the Weibull modulus

Weibull modulus (m)	Mean/x_0	Variance/x_0^2
0.5	2.0000	20.000
1.0	1.0000	1.000
2.0	0.8862	0.215
3.0	0.8934	0.105
3.5	0.8998	0.081
4.0	0.9064	0.065
5.0	0.9182	0.044
6.0	0.9275	0.033
10.0	0.9514	0.013
20.0	0.9730	0.004

$$F(x) = \frac{1}{n + 1} \quad \text{(Eq 20)}$$

where n is the total number of data points and i is the ith order in the ascending data set. An alternative value is the median rank value and is given as:

$$F(x) = \frac{i - 0.3}{n + 0.4} \quad \text{(Eq 21)}$$

The mean value is commonly used, because it represents the expected value of the distribution. However, in highly skewed distributions the median rank value may be a better choice. In addition to mean and median values, $F(x) = (i - 0.5)/n$ (Ref 113) and $(i - 0.375)/(n + 0.25)$ (Ref 114) have also been used. The effects of these four estimators have been discussed by Bergman (Ref 112).

4.3.2 Maximum Likelihood Method

A second method for obtaining Weibull parameters is the maximum likelihood method (Ref 115). The likelihood function, L, is the mathematical expression for the probability of obtaining the observed data. The log-likelihood function is obtained by taking the natural logarithm of the likelihood function, that is:

$$\ln L = n \ln m - nm \ln x_0 + \sum_{i=1}^{n} (m - 1) \ln x_i - \sum_{i=1}^{n} \left(\frac{x_i}{x_0}\right)^m \quad \text{(Eq 22)}$$

To find the values of m and x_0, which maximize the Weibull likelihood function, the log-likelihood function is differentiated with respect to m and x_0, the resulting expressions are equated to zero, and then m and x_0 can be solved simultaneously:

$$x_0 = \left[\frac{\sum_{i=1}^{n} (x_i)^m}{n}\right]^{1/m} \quad \text{(Eq 23)}$$

$$\frac{n}{m} + \sum_{i=1}^{n} \ln x_i - \sum_{i=1}^{n} (\ln x_i)\left(\frac{x_i}{x_0}\right)^m = 0 \qquad \text{(Eq 24)}$$

The Weibull parameters can be obtained by the maximum likelihood method through an iterative procedure. It is convenient to use the starting values obtained from the Weibull plots; the equation converge to within ±0.001 in a few steps.

4.3.3 Linear Estimation of Weibull Parameters

Linear estimators, as detailed below, are sometimes convenient for obtaining Weibull parameters (Ref 116). The linear estimators are

$$m = \sum_{i=1}^{n} a_i x_i \qquad \text{(Eq 25)}$$

$$x_0 = \sum_{i=1}^{n} c_i x_i \qquad \text{(Eq 26)}$$

where a_i and c_i are constant coefficients. However, there are no simple formulas giving a_i and c_i; thus, tables of coefficients must be constructed to estimate m and x_0 (Ref 116). Best linear unbiased estimators (i.e.,"b.l.u.e.'s," which means estimators with minimum variance in the class of linear unbiased estimators) can be obtained from general results on the linear estimation of Weibull parameters (Ref 117, 118). An alternative method, considered the minimum mean square error, is the best linear invariant estimators (b.l.i.e.'s), which is probably the most convenient for small- and moderate-size samples ($25 \leq n$) (Ref 119, 120). Both b.l.u.e.'s and b.l.i.e.'s require the evaluation of means, variances, and covariances; then Monte Carlo simulation is used to produce the desired tables. Tables of coefficients for linear estimators are available in Ref 117 to 120.

4.3.4 Nonlinear Least-Squares Estimation

Nonlinear curve fitting of the Weibull function has also been performed by least-squares estimation (Ref 111). These methods have been compared by Heavens and Murgatroyd (Ref 121).

4.4 *Confidence Intervals*

The numerical determination of m must be considered with errors associated in its generation; for example, a value of 2 ± 1 is probably not significantly different from a value of 5 ± 2. Confidence limits for Weibull parameters are usually developed by the application of Monte Carlo simulation. The pivotals of the Weibull distribution, Z_1 and Z_2, can be used to obtain confidence intervals for characteristic value x_0 and Weibull modulus m, respectively (Ref 116). The pivotals are defined as:

$$Z_1 = \frac{\tilde{x}_0 - x_0}{\tilde{m}} \qquad \text{(Eq 27)}$$

$$Z_2 = \frac{\tilde{m}}{m} \qquad \text{(Eq 28)}$$

For example, if l_2 and l_2 are such that $F(l_1 \leq Z_1 \leq l_2) = \alpha$, then $(\tilde{x}_o - l_2\tilde{m}, \tilde{x} - l_1\tilde{m})$ is the α confidence for x_0. Similarly, if $F(l_1 \leq Z_2 \leq l_2) = \alpha$, then $(\tilde{m} / l_2, \tilde{m} / l_1)$ is the α confidence for m. Any equivalent estimators of $\tilde{x}_0$ and $\tilde{m}$ can be used, but the properties of the intervals will depend strongly on the estimators. An alternative approach is to use Z_1, Z_2, and Z_p, where $Z_p = (\tilde{x}_o - \tilde{x}_p) / \tilde{m}$ and x_p is the pth quantile of the distribution (Ref 122, 123).

Various tables of percentage points for pivotals have been created by Monte Carlo simulation. Mann et al (Ref 124, 125) considered pivotals based on b.l.i.e.'s and gave tables of percentage points for Z_1, Z_2, and Z_p ($p = 0.001$, 0.005, and 0.10) for samples with $3 \leq n \leq 25$. Pivotals based on maximum likelihood estimation were developed (Ref 126). Thoman et al. (Ref 127) yielded percentage points for Z_1 and Z_2 for a sample size of 120.

Tables for pivotals are very difficult to produce, because a large amount of simulation is required for individual n and i (n, total number of data points; i, ith order in the ascending data set), and no tables cover all sample sizes that may be practically encountered. A simple approximation for the Z_2 distribution based on maximum likelihood estimation was utilized. This approximation involved the χ^2 distribution and was developed empirically (Ref 114). A special case for the application of the χ^2 distribution is called the likelihood ratio method and is a reasonably simple way to obtain confidence intervals. Recall the log-likelihood equation (Eq 22), and the likelihood ratio statistic, Λ, is given as:

$$\Lambda = -2 \ln[L(x_0,\tilde{m})] + 2 \ln [\tilde{L}(x_0,\tilde{m})] = \chi^2_{1,\alpha} \qquad \text{(Eq 29)}$$

$$\Lambda = -2 \ln[L(\tilde{x}_0,m)] + 2 \ln[L(\tilde{x}_0,\tilde{m})] = \chi^2_{1,\alpha} \qquad \text{(Eq 30)}$$

An approximate α confidence interval is obtained by finding the set of x_0 (lower and higher bounds) through iterative applications of Eq 29. Similarly, the set of m can be found by applying several iterations of Eq 30.

The processes to obtain confidence limits of Weibull parameters are sophisticated and mathematically intractable. For the commonly used confidence limits of 90, 95, and 99%, if the sample size is large and uncensored, the confidence intervals for x_0 and m can be approximated by maximum error estimation using Eq 31 and 32, respectively (Ref 128):

$$\tilde{x}_0 \exp\left(\frac{-1.05\, W_\alpha}{\tilde{m}\sqrt{n}}\right) \leq x_0 \leq \tilde{x}_0 \exp\left(\frac{1.05\, W_\alpha}{\tilde{m}\sqrt{n}}\right) \qquad \text{(Eq 31)}$$

$$\tilde{m} \exp\left(\frac{-0.78\, W_\alpha}{\sqrt{n}}\right) \leq m \leq \tilde{m} \exp\left(\frac{0.78\, W_\alpha}{\sqrt{n}}\right) \qquad \text{(Eq 32)}$$

where $W_{0.99} = 2.576$, $W_{0.95} = 1.960$, and $W_{0.90} = 1.645$.

In summary, the inhomogeneous structure of thermal spray coatings leads to a highly variable material property determination. This section has discussed mechanical properties of coat-

ings in terms of distribution functions. Thus, the estimation of error and confidence intervals becomes important.

5. Conclusions

The adhesion strength or cohesion strength of thermal spray coatings can be influenced by many factors. Some of these factors are intrinsic—that is, related to the spray variables, such as powder characteristics, spray parameters, and substrate preparation. Others are extrinsic, including post treatment and service conditions such as hot corrosion, thermal shock, and so on. However, adhesion tests are usually performed at room temperature and do not consider in-service conditions that may decrease adhesion strength. It is important for materials designers to keep in mind that adhesion strength is strongly related to service conditions. Also, the estimation of confidence intervals for such coatings enables the reliability of the so-determined property to be ascertained.

The measurement of the adhesion of thermal spray materials is, at least on the conceptual level, a routine operation. The tensile adhesion method detailed in ASTM C633 is simple and is often used in industry to rank different coatings. However, the major shortcoming of this test is that it does not promote any understanding of coating performance, that is, how coatings can be designed to be more functional. Thus, the present paper has addressed other methods based on fracture mechanics and mechanism-based studies.

The design of experiments with regard to material property optimization of coatings is another area of intense effort. Experimental protocols based on Taguchi and response surface methodology offer engineers efficient and viable means to optimize process parameters (Ref 129, 130). Such statistical methods are executed to discriminate key parameters that induce the variation of coating properties. The signal-to-noise ratios of the processing parameters are derived from such studies (Ref 131). The Taguchi method does have some shortcomings and limitations (Ref 132), but it is a simple and powerful process-control procedure.

The coating should be considered as one part of the overall system. Therefore, the current trend is to design the coating as an integral part of the component assembly rather than as an add-on to the substrate; this is termed a "prime reliant coating" in the aerospace and turbine engine industries. Although the property of coating adhesion to the substrate is of principal interest, there is still no single measurement that can satisfy all the requirements for determining material properties. Standardization of measurements, which may be achieved by improving existing experimental techniques or by combining two or more techniques, will aid future coating development.

Finally, a coating design (i.e., both microstructural and mechanical engineering designs) that is based on lifetime modeling is the critical information that should be forthcoming from any test method. Such designs will increase understanding of thermal sprayed materials and coatings so that their reliability and application will grow.

ACKNOWLEDGMENTS

This work has received partial support from the Alcoa Foundation, and the authors thank P. Fussell and R. Kaufold for their management of this program. The research program has also been supported by the National Science Foundation under the STRATMAN Program DDM 9215846.

References

1. T.N. Rhys Jones, Thermally Sprayed Coating Systems for Surface Protection and Clearance Control Application in Aero Engines, *Surf. Coat. Technol.*, Vol 43/44, 1990, p 402-415
2. K.T. Scott and R. Kingswell, Thermal Spraying, *Advanced Surface Coatings*, D.S. Rickerby and A. Mattews, Ed., Chapman and Hall, 1991, p 217-243
3. J.H. Zatt, A Quarter of a Century of Plasma Spraying, *Annual Review of Material Science*, Vol 13, R.A. Huggins, R.H. Bube, and D.A. Vermilyea, Ed., Annual Review Inc., 1983, p 9-42
4. C.C. Berndt, Ed., *Thermal Spray: International Advances in Coatings Technology*, ASM International, 1992
5. C.C. Berndt and T.F. Bernecki, Ed., *Thermal Spray Coatings: Research, Design and Application*, ASM International, 1993
6. S. Blum-Sandmeier, H. Eschnauer, P. Huber, and A.R. Nicoll, Ed., *Proc. 2nd Plasma-Technik-Symp.*, Plasma-Technik AG, Wohlen/Switzerland, Häfliger Druck AG, Wettingen, 1991
7. L.E. Weiss, F.B. Prinz, D.A. Adams, and D.P. Siewiorek, Thermal Spray Shape Deposition, *J. Therm. Spray Technol.*, Vol 1(No. 3), 1992, p 231-237
8. K. Neufuss, B. Kolman, J. Dubsky, and P. Chraska, Plasma Sprayed Free-Standing Ceramic Parts, *Proc. AustCeram 92* (Melbourne), 16-21Aug 1992, p 124-129
9. R. McPherson, A Review of Microstructure and Properties of Plasma Sprayed Ceramic Coatings, *Surf. Coat. Technol.*, Vol 39/40, 1989, p 173-181
10. V.H.S. Wilms, "The Microstructure of Plasma Sprayed Ceramic Coatings," Ph.D. thesis, SUNY at Stony Brook, 1978
11. K.L. Mittal, "Adhesion Measurement: Recent Progress, Unsolved Problems, and Prospects," *Adhesion Measurement of Thin Films, Thick Films, and Bulk Coatings*, STP 640, K.L. Mittal Ed., ASTM, 1978 p5-17
12. K.L. Mittal, Ed., *Adhesion Measurement of Thin Films, Thick Films, and Bulk Coatings*, STP 640, ASTM, 1978
13. R.L. Patrick, *Treatise on Adhesion and Adhesive*, Vol 1, Marcel Dekker, 1967
14. "Standard Terminology of Adhesives," D 907-82, *Annual Book of Standards*, Vol 15.06, ASTM, 1985, p 45-54
15. J. Comyn, Surface Treatment and Analysis for Adhesive Bonding, *Int. J. Adhes. Adhes.*, Vol 10 (No. 3), 1990, p 161-165
16. A. Matting and H.-D. Steffens, Adherence and Coating by Arc Spraying and Flame Spraying, Parts 1-3, *Metallwiss. Tech.*, Vol 17, 1963, p 583-593, 905-922, 1213-1230
17. M.D. Thouless, The Role of Fracture Mechanics in Adhesion, *Mater. Res. Soc. Symp. Proc.*, Vol 119, 1988, p 51-62
18. B.R. Lawn and T.R. Wilshaw, *Fracture of Brittle Solids*, Cambridge University Press, 1975
19. C.C. Berndt and R. McPherson, A Fracture Mechanics Approach to the Adhesion of Flame and Plasma Sprayed Coatings, *Trans. Int. Eng.*, Vol 6 (No. 4), 1981, p 53-58
20. C.C. Berndt, Fracture Toughness Tests on Plasma Sprayed Coatings, *Advances in Fracture Research*, Vol 4, S.R. Valluri, D.M.R. Taplin, P. Rama Rao, J.F. Knott, and R. Dubey, Ed., Pergamon Press, Oxford, 1984, p 2545-2552
21. G.N. Heintze and R. McPherson, Fracture Toughness of Plasma Sprayed Zirconia Coatings, *Surf. Coat. Technol.*, Vol 34, 1988, p 15-23
22. C.C. Berndt, "The Adhesion of Flame and Plasma Sprayed Coatings," Ph.D. thesis, Monash University, Clayton, Victoria, Australia, 1980

23. P. Ostojic, "The Adhesion of Thermally Sprayed Coatings," Ph.D. thesis, Monash University, Clayton, Victoria, Australia, 1986
24. K.L. Mittal, Selected Bibliography on Measurement of Films and Coatings, *J. Adhes. Sci. Technol.*, Vol 1(No. 3), 1987, p 247-259
25. D.S. Rickerby, A Review of the Methods for the Measurement of Coating-Substrate Adhesion, *Surf. Coat. Technol.*, Vol 36, 1988, p 541-557
26. S.J. Bull and D.S. Rickerby, Evaluation of Coatings, *Br. Ceram. Trans. J.*, Vol 88, 1989, p 177-183
27. P.R. Chalker, S.J. Bull, and D.S. Rickerby, A Review of the Methods for the Evaluation of Coating-Substrate Adhesion, *Mater. Sci. Eng.*, Vol A140, 1991, p 583-592
28. B.A. Lyashenko, V.V. Rishin, V.G. Zil'berberg, and S.Yu. Sharivker, Strength of Adhesion Between Plasma-Sprayed Coatings and the Base Metal, *Sov. Powder Metall. Met. Ceram.*, Vol 8, 1969, p 331-334
29. B.M. Zakharov, M.G. Trofimov, L.I. Guseva, Y.I. Golovkin, A.A. Kononov, and V.V. Vinokurova, Bond Strength of Coatings Applied by the Flame Plating Technique, *Sov. Powder Metall. Met. Ceram.*, Vol 9, 1970, p 925-929
30. W.E. Stanton, The Mechanical Properties of Sprayed Metals for Engineering, *7th Int. Metal Spraying Conf.*, The Welding Institute, Cambridge, U.K., 1974, p 157-164, 312-314
31. T. Suhara, K. Kitajima, and S. Fukada, Coatings by Wire Explosion Spraying—Properties and Applications, *7th Int. Metal Spraying Conf.*, The Welding Institute, Cambridge, U.K., 1974, p 179-184
32. N.N Rykalin, Plasma Engineering in Metallurgy and Inorganic Materials Technology, *Pure Appl. Chem.*, Vol 48, 1976, p 179-194
33. V.E. Belashchenko and Y.B. Chernyak, Stochastic Approach to the Modeling of Thermal Spray Coating Formation, *Thermal Spray: International Advances in Coatings Technology,* C.C. Berndt, Ed., ASM International, 1992, p 433-437
34. R.L. Apps, New Developments in Ceramics and Coatings, *Chem. Eng. (UK)*, Vol 292, 1974, p 769-773
35. V. Wilms and H. Herman, Plasma Spraying of Al_2O_3 and Al_2O_3-Y_2O_3, *Thin Solid Films*, Vol 39, 1976, p 251-262
36. T.J. Steeper, D.J. Varacalle, Jr., G.C. Wilson, W.L. Riggs II, A.J. Rotolico, and J.E. Nerz, A Design of Experiment Study of Plasma Sprayed Alumina-Titania Coatings, *Thermal Spray: International Advances in Coatings Technology,* C.C. Berndt, Ed., ASM International, 1992, p 415-420
37. C.C. Berndt, Tensile Adhesion Testing Methodology for Thermally Sprayed Coatings, *J. Mater. Eng.*, Vol 12, 1990, p 151-158
38. Y. Shimizu, M. Sato, M. Kobayashi, and K. Maeda, Effect of Test Specimen Size upon Adhesive Strength of Flame Sprayed Coatings, *Thermal Spray: International Advances in Coatings Technology,* C.C. Berndt, Ed., ASM International, 1992, p 257-262
39. W. Han, E.F. Rybicki, and J.R. Shadley, An Improvement Specimen Geometry for ASTM C633-79 to Estimate Bond Strength of Thermal Spray Coatings, *J. Therm. Spray Technol.*, Vol 2 (No. 2), 1993, p 145-150
40. W. Han, E.F. Rybicki, and J.R. Shadley, Application of Fracture Mechanics to the Interpretation of Bond Strength Data from ASTM Standard C633-79, *J. Therm. Spray Technol.*, Vol 2 (No. 3), 1993, p 235-241
41. G.E. Dieter, in *Mechanical Metallurgy*, McGraw-Hill, 1988, p 348-374
42. F.J. Hermanek, Determining the Adhesive/Cohesive Strength of Thin Thermally Sprayed Deposits, *Weld. J.*, Vol 57, 1978, p 31-35
43. C.C. Berndt, Tensile Adhesion Test Measurements on Plasma-Sprayed Coatings, *Advances in Fracture Research*, Vol 4, S.R. Valluri, D.M.R. Taplin, P. Rama Rao, J.F. Knott, and R. Dubey, Ed., Pergamon Press, Oxford, 1984, p 2553-2559
44. P.F. Becher and W.L. Newell, Adherence-Fracture of Glass-Bonded Thick-Film Conductor: Effect of Firing Conditions, *J. Mater. Sci.*, Vol 12, 1977, p 90-96
45. P.F. Becher, W.L. Newell, and S.A. Halen, Application of Fracture Mechanics to the Adherence of Thick Films and Ceramic Braze Joints, *Fracture Mechanics of Ceramics,* Vol III, R.C. Bradt, D.P.H. Hasselman, and F.F. Lange, Ed., Plenum Press, 1978, p 463-471
46. W.D. Bascom and J.L. Bitner, A Fracture Approach to Thick Film Adhesion Measurements, *J. Mater. Sci.*, Vol 12, 1977, p 1401-1410
47. S. Mostovoy, P.B. Crosley, and E.J. Ripling, Use of Crack-Line-Loaded Specimens for Measuring Plane-Strain Fracture Toughness, *J. Mater.*, Vol 2, 1967, p 661-681
48. G.N. Heintze and R. McPherson, A Further Study of the Fracture Toughness of Plasma-Sprayed Zirconia Coatings, *Surf. Coat. Technol.*, Vol 36, 1988, p 125-132
49. J.O. Outwater and D.J. Gerry, On the Fracture Energy, Rehealing Velocity and Refracture Energy of Cast Epoxy Resin, *J. Adhes.*, Vol 1, 1969, p 290-298
50. J.A. Kies and A.B.J. Clark, Fracture Propagation Rates and Times to Fail Following Proof Stress in Bulk Glass, *Fracture 1969*, P.L. Pratt, Ed., Chapman and Hall, London, 1969, p 483-491
51. M.K. Ferber and S.D. Brown, Delayed Failure of Plasma-Sprayed Al_2O_3 Applied to Metallic Substrates, *J. Am. Ceram. Soc.*, Vol 64 (No. 12), 1981, p 737-743
52. L.C. Cox, The Four-Point Bend Test as a Tool for Coating Characterization, *Surf. Coat. Technol.*, Vol 36, 1988, p 807-815
53. S.J. Howard and T.W. Clyne, Interfacial Fracture Toughness of Vacuum-Plasma-Sprayed Coatings, *Surf. Coat. Technol.*, Vol 45, 1991, p 333-342
54. A.G. Evans, Fracture Mechanics Determinations, *Fracture Mechanics of Ceramics,* Vol 1, R.C. Bradt, D.P.H. Hasselman, and F.F. Lange, Ed., Plenum Press, 1974, p 17-48
55. P. Benjamin and C. Weaver, Measurement of Adhesion of Thin Film, *Proc. R. Soc. (London) A*, Vol 254, 1960, p 163-176
56. A.J. Perry, J. Valli, and P.A. Steinmann, Adhesion Scratch Testing: A Round-Robin Experiment, *Sur. Coat. Technol.*, Vol 36, 1988, p 559-575
57. C. Julia-Schmutz and H.E. Hintermann, Microscratch Testing to Characterize the Adhesion of Thin Layers, *Surf. Coat. Technol.*, Vol 48, 1991, p 1-6
58. P.J. Burnett and D.S. Rickerby, The Relationship Between Hardness and Scratch Adhesion, *Thin Solid Films*, Vol 154, 1987, p 403-416
59. S.J. Bull, D.S. Rickerby, A. Matthews, A. Leyland, A.R. Pace, and J. Valli, The Use of Scratch Adhesion Testing for the Determination of Interfacial Adhesion: The Importance of Frictional Drag, *Surf. Coat. Technol.*, Vol 36, 1988, p 503-517
60. J. Sekler, P.A. Steinmann, and H.E. Hintermann, The Scratch Test: Different Critical Load Determination Techniques, *Surf. Coat. Technol.*, Vol 36, 1988, p 519-529
61. S.J. Bull, Failure Modes in Scratch Adhesion Testing, *Surf. Coat. Technol.*, Vol 50, 1991, p 25-32
62. D.K. Das, M.P. Srivastava, S.V. Joshi, and R. Sivakumar, Scratch Adhesion Testing of Plasma-Sprayed Yttria-Stabilized Zirconia Coatings, *Surf. Coat. Technol.*, Vol 46, 1991, p 331-345
63. C.W. Anderson and K.H. Heffner, Precision Gas Bearing Plasma Sprayed Aluminum Oxide Coating Characterization, *Thermal Spray: International Advances in Coatings Technology,* C.C. Berndt, Ed., ASM International, 1992, p 695-704
64. M. Gudge, D.S. Rickerby, R. Kingswell, and K.T. Scott, Residual Stress in Plasma Metallic and Ceramic Coatings, *Thermal Spray Research and Application*, T.F. Bernecki, Ed., ASM International, USA, 1991, p 331-337
65. E. Lopez, F. Beltzung, and G. Zambelli, Measurement of Cohesion and Adhesion Strengths in Alumina Coatings Produced by Plasma Spraying, *J. Mater. Sci. Lett.*, Vol 8, 1989, p 346-348

66. F. Beltzung, G. Zambelli, E. Lopez, and A.R. Nicoll, Fracture Toughness Measurement of Plasma Sprayed Ceramic Coatings, *Thin Solid Films*, Vol 181, 1989, p 407-415
67. M.J. Noone and R.L. Mehan, Observation of Crack Propagation in Polycrystalline Ceramics and Its Relationship to Acoustic Emission, *Fracture Mechanics of Ceramics*, Vol 1, R.C. Bradt, D.P.H. Hasselman, and F.F. Lange, Ed., Plenum Press, 1974, p 201-229
68. R.G. Liptai, D.O. Harris, and C.A. Tatro, *Acoustic Emission*, STP 505, ASTM, 1972
69. J.R. Matthews, *Acoustic Emission*, Gordon & Breach, 1983
70. T.C. Nerz, J.E. Nerz, B.A. Kushner, A.J. Rotolico, and W.L. Riggs, Evaluation of HEP Sprayed Tungsten Carbide/Cobalt Coating Using Design of Experiment Method, *Thermal Spray: International Advances in Coatings Technology*, C.C. Berndt, Ed., ASM International, 1992, p 405-414
71. M.M Mayuram and R. Krishnamurphy, Some Studies on Acoustic Emission Application in Assessing Tribological Characteristics of Plasma Sprayed Ceramic Coatings, *Thermal Spray: International Advances in Coatings Technology*, C.C. Berndt, ASM International, 1992, p 711-715
72. N. Iwamoto, M. Kamai, and G. Ueno, Examination of Tungsten Carbide Coatings for Thermal Cycling Using NDT, *Thermal Spray: International Advances in Coatings Technology*, C.C. Berndt, Ed., ASM International, 1992, p 259-265
73. H. Nakahira, Y. Harada, N. Mifune, T. Yogoro, and H. Yamane, Advanced Thermal Barrier Coatings Involving Efficient Vertical Micro-Cracks, *Thermal Spray: International Advances in Coatings Technology*, C.C. Berndt, Ed., ASM International, 1992, p 519-524
74. H.L. Dunegan, Quantitative Capabilities of Acoustic Emission for Predicting Structural Failure, *Prevention of Structural Failure*, American Society for Metals, 1975, p 86-113
75. T. Tsuru, A. Sagara, and S. Haruyama, Acoustic Emission Measurements to Evaluate the Degradation of Coating Films, *Corrosion*, Vol 43 (No. 11), 1987, p 703-707
76. F. Bordeaux, C. Moreau, and R.G. Saint Jacques, Acoustic Emission Study of Failure Mechanisms in TiC Thermal Barrier Coatings, *Surf. Coat. Technol.*, Vol 54/55, 1992, p 70-76
77. C.C. Berndt, Failure Processes Within Ceramic Coatings at High Temperatures, *J. Mater. Sci.*, Vol 24, 1989, p 3511-3520
78. I.G. Scott, *Basic Acoustic Emission*, Gordon & Breach, 1991
79. C.C. Berndt and R.A. Miller, Failure Analysis of Plasma-Sprayed Thermal Barrier Coatings, *Thin Solid Films*, Vol 119, 1984, p 173-184
80. C.C. Berndt, Examination of Coating Failure by Acoustic Emission, *Thermal Barrier Coatings Workshop*, NASA Lewis Research Center, Cleveland, 21-22 May, 1985, p 127-137
81. H.-D. Steffens and H.-A. Crostack, Non-Destructive Testing of Thermally Sprayed Coatings, *General Aspects of Thermal Spraying*, J.H. Zaat, Ed., The Hague, Netherlands, 1980, p 120-128
82. K. Hoehne, Moeglichkeiten der zerstoerungsfreien Prunfung von Metallspritzschichten, Schweisstechnik, Vol 13, 1963, p 55-61
83. W. Francke and A.W.J. de Gee, A Non-Destructive Method for the Measurement of the Adhesive Bond Strength of Thermally Sprayed Nonfused Coatings, *Proc. Int. Conf. Advances in Surface Technology*, London, 1978, p 99-109
84. R.L. Cox, D.P. Almond, and H. Reiter, Ultrasonic Studies of Plasma Sprayed Coatings, *General Aspects of Thermal Spraying*, J.H. Zaat, Ed., The Hague, Netherlands, 1980, p 133-137
85. Y. Suga, Harjanto, and J. Takahashi, Study on the Ultrasonic Test for Evaluating the Adhesion of Sprayed Coatings to a Substrate, *Thermal Spray: International Advances in Coatings Technology*, C.C. Berndt, Ed., ASM International, 1992, p 247-252
86. E. Lugscheider, P. Jokiel, G. Purshe, O. Roman, and K. Yushchenko, Particle Reinforced Material Containing Titanium-I-Boride for Wear Protection, *Thermal Spray: International Advances in Coatings Technology*, C.C. Berndt, Ed., ASM International, 1992, p 647-651
87. K. Furukubo, S. Oki, and S. Gohda, Relationship Between Wear and Microstructures of Ceramic Spray Coatings, *Thermal Spray: International Advances in Coatings Technology*, C.C. Berndt, Ed., ASM International, 1992, p 705-709
88. R.C. Hendricks and G. McDonald, "Assessment of Variations in Thermal Cycle Life Date of Thermal Barrier Coated Rods," TM-81743, NASA, Cleveland, 1981
89. H.-D. Steffens and U. Fischer, Characterization and Thermal Shock Testing of Yttria-Stabilized Zirconia Coatings, *Surf. Coat. Technol.*, Vol 32, 1987, p 327-338
90. S.J. Grisaffe, "Analysis of Shear Bond Strength of Plasma-Sprayed Alumina Coatings on Stainless Steel," TN D3113, NASA, Cleveland, 1965
91. H. Grützner and H. Weiss, A Novel Shear Test for Plasma-Sprayed Coatings, *Surf. Coat. Technol.*, Vol 45, 1991, p 317-323
92. K.K. Schweitzer, M.H. Zeihl, and Ch. Schwaminger, Improved Methods for Testing Bond and Intrinsic Strength and Fatigue of Thermally Sprayed Metallic and Ceramic Coatings, *Surf. Coat. Technol.*, Vol 48, 1991, p 103-111
93. M.J. Filiaggi and R.M. Pilliar, Mechanical Testing of Plasma-Sprayed Ceramic Coatings on Metal Substrates: Interfacial Fracture Toughness and Tensile Bond Strength, *J. Mater. Sci.*, Vol 26, 1991, p 5383-5395
94. H.R. Brown and A.C.M. Yang, The Use of Peel Test to Examine the Self Adhesion of Polyimide Films, *J. Adhes. Sci. Technol.*, Vol 6 (No. 3), 1992, p 333-346
95. M. Mantel and F. Descaves, Study of a T-Type Peel Test on a Metal/Polymer/Metal Sheet Sandwich, *J. Adhes. Sci. Technol.*, Vol 6 (No. 3), 1992, p 357-376
96. B. Lawn and R. Wilshaw, Review—Indentation Fracture: Principles and Applications, *J. Mater. Sci.*, Vol 10, 1975, p 1049-1081
97. H.R. Hertz, *Hertz's Miscellaneous Papers*, MacMillian Press, London, 1882, chap. 5,6
98. B.R. Lawn and D.B. Marshall, Indentation Fracture and Strength Degradation in Ceramics, *Fracture Mechanics of Ceramics*, Vol 3, R.C. Bradt, D.P.H. Hasselman, and F.F. Lange, Ed., Plenum Press, 1978, p 205-229
99. P. Ostojic and R. McPherson, Indentation Toughness Testing of Plasma Sprayed Coatings, *Mater. Forum*, Vol 10 (No. 4), 1987, p 247-255
100. J.G. Binner and R. Stevens, The Measurement of Toughness by Indentation, *Trans. J. Br. Ceram. Soc.*, Vol 83, 1984, p 168-172
101. C. Richard, J. Lu, J.F. Flavenot, G. Beranger, and F. Decomps, Study of Cr_2O_3 Coating Materials and Characterization by an Interfacial Test of Coating/Substrate Adherence, *Thermal Spray: International Advances in Coatings Technology*, C.C. Berndt, Ed., ASM International, 1992, p 11-16
102. R. Dal Maschio, V.M. Sgavo, L. Bertamini, and E. Galvanetto, Measurement of Metal-Ceramic Adhesion by Indentation Technique in Thick TBCs, *Thermal Spray: International Advances in Coatings Technology*, C.C. Berndt, Ed., ASM International, 1992, p 947-951
103. C.C. Berndt, J. Karthikeyan, R. Ratanaraj, and Yang Da Jun, Material Property Variations in Thermally Sprayed Coatings, *Thermal Spray Coatings: Properties, Processes, and Applications*, T.F. Bernecki, Ed., ASM International, 1992, p 199-203
104. C.C. Berndt, J. Ilavsky, and J. Karthikeyan, Microhardness-Lifetime Correlations for Plasma Sprayed Thermal Barrier Coatings, *Thermal Spray: International Advances in Coatings Technology*, C.C. Berndt, Ed., ASM International, 1992, p 941-946
105. C.K. Lin and C.C. Berndt, Microhardness Variation in Thermally Sprayed Coatings, *Thermal Spray Coatings: Research, Design and Application*, C.C. Berndt and T.F. Bernecki, Ed., ASM International, 1993, p 561-568

106. R.A. Miller, Oxidation-Based Model for Thermal Barrier Coating Life, *J. Am. Ceram. Soc.*, Vol 67 (No. 8), 1984, p 517-521
107. W. Weibull, A Statistical Theory of the Strength of Materials, *Ingeniorsvetenskapakademiens. Handlinger Nr.*, Vol 151, 1939
108. S.B. Batdorf, Fundamentals of the Statistical Theory of Fracture, *Fracture Mechanics of Ceramics*, Vol 3, R.C. Bradt, D.P.H. Hasselman, and F.F. Lange, Ed., Plenum Press, 1978, p 1-30
109. W. Weibull, A Statistical Distribution Function of Wide Applicability, *J. Appl. Mech.*, Sept 1951, p 293-297
110. K.C. Kapur and L.R. Lamberson, *Reliability in Engineering Design*, John Wiley & Sons, 1977
111. D.G.S. Davies, The Statistical Approach to Engineering Design in Ceramics, *Proc. Br. Ceram. Soc.*, 1973, p 429-452
112. B. Bergman, On the Estimation of the Weibull Modulus, *J. Mater. Sci. Lett.*, Vol 3, 1984, p 689-692
113. K. Trustrum and A. DE S. Jayatilaka, On Estimating the Weibull Modulus for a Brittle Material, *J. Mater. Sci.*, Vol 14, 1979, p 1080-1084
114. J.S. White, The Moments of Log-Weibull Order Statistics, *Technometrics*, Vol 11 (No. 2), 1969, p 373-386
115. A.C. Cohen, Maximum Likelihood Estimation in the Weibull Distribution Based on Complete and on Censored Samples, *Technometrics*, Vol 7 (No. 4), 1965, p 579-588
116. J.F. Lawless, in *Statistical Models and Methods for Lifetime Data*, John Wiley & Sons, 1982, p 141-202
117. E.H. Lloyd, Least-Squares Estimation of Location and Scale Parameters Using Order Statistics, *Biometrika*, Vol 39, 1952, p 88-95
118. M.G. Kendall and A. Stuart, *The Advanced Theory of Statistics*, Vol 2, 2nd ed., Griffin, London, 1969
119. N.R. Mann, Table for Obtaining the Best Linear Invariant Estimates of Parameters of the Weibull Distribution, *Technometrics*, Vol 9, 1967, p 629-645
120. N.R. Mann, "Results on Location and Scale Parameter Estimation with Application to the Extreme Value Distribution," ARL 67-0023, Wright-Patterson Air Force Base, 1967
121. J.W. Heavens and P.N. Murgatroyd, Analysis of Brittle Fracture Stress Statistics, *J. Am. Ceram. Soc.*, Vol 53 (No. 9), 1970, p 503-505
122. R.A. Fisher, Two New Properties of Mathematical Likelihood, *Proc. R. Soc. (London) A.*, Vol 144, 1934, p 285-307
123. J.F. Lawless, Confidence Interval Estimation for the Weibull and Extreme Value Distributions, *Technometrics*, Vol 20, 1978, p 355-364
124. N.R. Mann, K.W. Fertig, and E.M. Scheuer, "Confidence and Tolerance Bounds and a New Goodness of Fit Test for the Two-Parameter Weibull or Extreme Value Distribution with Tables for Censored Samples of Size 3(1)25," ARL 71-0077, Wright-Patterson Air Force Base, 1971
125. N.R. Mann and K.W. Fertig, Tables for Obtaining Confidence Bounds and Tolerance Bounds Based on Best Linear Invariant Estimates of Parameters of the Extreme Value Distribution, *Technometrics*, Vol 15, 1973, p 87-101
126. L.J. Bain, *Statistical Analysis of Reliability and Life-Testing Models*, Marcel Dekker, 1978
127. D.R. Thoman, L.J. Bain, C.E. Antle, Inference on the Parameters of the Weibull Distribution, *Technometrics*, Vol 11, 1969, p 445-460
128. R.B. Abernethy, J.E. Breneman, C.H. Medlin, and G.L. Reinman, *Weibull Analysis Handbook*, AFWAL-TR-83-2079, Propulsion Laboratory, Air Force Wright Aeronautical Laboratories, Wright-Patterson Air Force Base, 1983
129. G. Taguchi and S. Konishi, *Taguchi Methods, Orthogonal Arrays and Linear Groups*, American Supplier Institute, 1987
130. P. Ross, *Taguchi Techniques for Quality Engineering*, McGraw-Hill, 1988
131. G.E.P. Box, Signal to Noise Ratios: Performance Criteria and Transformation, *Technometrics*, Vol 30 (No. 1), 1988, p 1-17
132. S. Bisgaard, Optimizing Thermal Spray Processes Going Beyond Taguchi Methods, *Thermal Spray Research and Application*, T.F. Bernecki, Ed., ASM International, 1991, p 661-667